Annex No. 2b.
Self presentation in English

Dr Jacek Rzadkiewicz
Radiation Detectors and Plasma Diagnostic Division (TJ3)
National Centre for Nuclear Research (NCBJ), Otwock, 2019

<u>Contents</u>

1. Name
Jacek Rzadkiewicz

2. Degrees and diplomas awarded

PhD	2004	Institute for Nuclear Studies (currently, National Centre for Nuclear Research, NCBJ), Dissertation (with merit): "Precise x-ray spectroscopy of mid-Z multiply ionized atoms in inner electron shells." under the supervision of Prof. Ziemowid Sujkowski.
The Master of Physics degree	1997	Warsaw University, Division of Nuclear Spectroscopy, Master's Thesis Title: "Interaction of oxygen ions with gold nuclei." under the supervision of Dr Jerzy Szerypo.

3. Professional experience

2012-2019	National Centre for Nuclear Research (NCBJ), adiunctus, in the Department of Nuclear Techniques and Equipment
2008-2012	Joint European Torus (JET) experimental thermonuclear reactor, Oxfordshire, Great Britain, a responsible officer of a high-resolution x-ray diagnostics
2005-2008	Institute for Nuclear Studies, adiunctus
2004-2005	GSI, Darmstadt, Germany, a postdoc in Prof. Thomas Stöhlker's atomic physics group
1999-2000	University of Fribourg, Switzerland, a recipient of a doctoral scholarship from the Government of the Swiss Federation, Prof. Jean-Claude Douss's atomic physics group
1997-2004	Institute for Nuclear Studies, a doctoral student in Prof. Ziemowid Sujkowski's atomic physics group

4. Indication of the achievement* of the requirements resulting from Article 16 (2) of the Act of 14 March 2003 on scientific degrees, academic titles and degrees and titles in art (Journal of Laws, 2016, item 882, as amended in Journal of Laws, 2016, item 1311.)

The title of the scientific achievement:
"Development of methods for analysis of high resolution x-ray spectra arising in collisions, stopping and plasma structures, and designing the conditions for observing the process of nuclear excitation by electron capture."

4.1 . List of publications being the basis of the habilitation procedure (list A)

[A1] **J. Rzadkiewicz**, Th. Stöhlker, D. Banaś, H. F. Beyer, F. Bosch, C. Brandau, C. Z. Dong, S. Fritzsche, A. Gojska, A. Gumberidze, S. Hagmann, D. C. Ionescu, C. Kozhuharov, T. Nandi, R. Reuschl, D. Sierpowski, U. Spillmann, A. Surzhykov, S. Tashenov, M. Trassinelli, S. Trotsenko, **Selective population of the [1s2s] $^1S_0$ and [1s2s] $^3S_1$ states of He-like uranium**, **Physical Review A 74** (2006) 012511.
IF*=3,047

[A2] **J. Rzadkiewicz**, O. Rosmej, A. Blazevic, V.P. Efremov, A. Gójska, D.H.H. Hoffmann, S. Korostiy, M. Polasik, K. Słabkowska, A.E. Volkov, **Studies of the Kα x-ray spectra of low-density SiO_2 aerogel induced by Ca projectiles for different penetration depths**, **High Energy Density Physics 3** (2007) 233.
IF*=1,68

[A3] J.-J. Wan, Ch.-Z. Dong, X.-B. Ding, X.-W. Ma, **J. Rzadkiewicz**, Th. Stöhlker, S. Fritzsche, **Radiative electron capture and subsequent radiative decay in collisions of U^{89+} ions with N_2**, **Physical Review A 79** (2009) 022707.
IF*=2,866

[A4] **J. Rzadkiewicz,** A. Gojska, O. Rosmej, M. Polasik, K. Słabkowska, **Interpretation of the Si Kα x-ray spectra accompanying the stopping of swift Ca ions in low-density SiO_2 aerogel**, **Physical Review A 82** (2010) 012703.
IF*=2,861

[A5] M. Polasik, K. Słabkowska, **J. Rzadkiewicz**, K. Kozioł, J. Starosta, E. Wiatrowska-Kozioł, J-Cl. Dousse, J. Hoszowska, **$K^h\alpha_{1,2}$ X-ray Hypersatellite Line Broadening as a Signature of K-Shell Double Photoionization Followed by Outer-Shell Ionization and Excitation**, **Physical Review Letters 107** (2011) 073001.
IF*=7,37

[A6] **J. Rzadkiewicz**, W. Dominik, M. Scholz, M. Chernyshova, T. Czarski, H. Czyrkowski, R. Dabrowski, K. Jakubowska, L. Karpinski, G. Kasprowicz, K. Kierzkowski, K. Pozniak, Z. Salapa, W. Zabolotny, P. Blanchard, S. Tyrrell, K.-D. Zastrow, **Design of T-GEM detectors for X-ray diagnostics on JET**, **Nucl. Instrum. Methods A 720** (2013) 36.
IF*=1,316

[A7] A. E. Shumack, **J. Rzadkiewicz**, M. Chernyshova, K. Jakubowska, M. Scholz, A. Byszuk, R. Cieszewski, T. Czarski, W. Dominik, L. Karpinski, G. Kasprowicz,

K. Pozniak, A. Wojenski, W. Zabolotny, N. J. Conway, S. Dalley, J. Figueiredo, T. Nakano, S. Tyrrell, K.-D. Zastrow, V. Zoita, JET EFDA Contributors, **X-ray crystal spectrometer upgrade for ITER-like wall experiments at JET**, **Review of Scientific Instruments 85** (2014) 11E425.
IF*=1,614

[A8] K. Słabkowska, **J. Rzadkiewicz**, Ł. Syrocki, E. Szymańska, A. Shumack, M. Polasik, N.R. Pereira, JET contributors, **On the interpretation of high-resolution x-ray spectra from JET with an ITER-like wall, Journal of Physics B: At. Mol. Opt. Phys. 48** (2015) 144028.
IF*=1,833

[A9] K. Kozioł, **J. Rzadkiewicz**, **Theoretical determination of two-electron one-photon transition characteristics for low-Z K-shell hollow atoms, Physical Review A 96**, (2017) 031402(R).
IF*=2,909

[A10] M. Polasik, K. Słabkowska, J.J. Carroll, C.J. Chiara, Ł. Syrocki, E. Węder, **J. Rzadkiewicz**, **Resonance conditions for ^{93m}Mo isomer depletion via nuclear excitation by electron capture in a beam-based scenario, Physical Review C 95** (2017) 034312.
IF*=3,304

[A11] C.J. Chiara, J.J. Carroll, M.P. Carpenter, J.P. Greene, D.J. Hartley, R.V.F. Janssens, G.J. Lane, J.C. Marsh, D.A. Matters, M. Polasik, **J. Rzadkiewicz**, D. Seweryniak, S. Zhu, S. Bottoni, A.B. Hayes, S.A. Karamian, **Isomer depletion as experimental evidence of nuclear excitation by electron capture, Nature 554** (2018) 216.
IF*=41,577

[A12] **J. Rzadkiewicz**, Y. Yang, K. Kozioł, M.G. O'Mullane, A. Patel, J. Xiao, K. Yao, Y. Shen, D. Lu, R. Hutton, Y. Zou, JET Contributors, **High-resolution tungsten spectroscopy relevant to the diagnostic of high-temperature tokamak plasmas, Physical Review A 97** (2018) 052501.
IF*=2,909

[A13] K. Kozioł, **J. Rzadkiewicz**, **MCDF-CI study of 4d − 3p X-ray transitions in Cu- and Ni-like tungsten ions, Physical Review A 98** (2018) 062504.
IF*=2,909

[A14] **J. Rzadkiewicz**, M. Polasik, K. Słabkowska, Ł. Syrocki, E. Węder, J.J. Carroll, C.J. Chiara, **Beam-based scenario for ^{242m}Am isomer depletion via nuclear excitation by electron capture**, **Physical Review C** 99 (2019) 044309.
IF*=3,304

Totlal IF* for publications [A1] – [A14] = 79.50
**Impact Factor*

4.2. Purpose and relevance of the studies

The rise of atomic physics dates back to 1913, when Niels Bohr proposed the first model of the atom. It was presented as a small (pointwise), dense and positively charged nucleus surrounded by electrons in the orbit. Despite exceeding slightly only a century, the history of atomic physics was full of exciting discoveries and amazing turns of events. In particular, atomic physics supported quantum physics, which allowed to verify and develop

subsequent quantum concepts. That is, for instance, quantum electrodynamics (QED), correlations of multiple bodies or parity non-conservation in atomic transitions due to weak interactions. Atomic physics, and high-resolution x-ray spectroscopy in particular, has been widely applied in many areas, from plasma diagnostics to the studies on stopping dynamics or material analysis. Development of atomic physics also prompted construction of new experimental devices such as storage rings, electron beam ion traps (EBIT), synchrotrons or free electron lasers.

It is also worth mentioning that the rapid development of atomic physics was accompanied by no less intense development of nuclear physics. Furthermore, over the last decades it has been discovered that some nuclear processes directly determine atomic transitions. As an example of such a process can serve inner conversion, due to which nuclear de-excitation with a simultaneous electron knockout from a given K, L or higher atomic shell. On the other hand, nuclear excitation by electron capture to an unfilled K, L or higher shell occur upon the reverse process to inner conversion. The strength of the nuclear process is in this case determined by atomic processes.

A particular area of interest for atomic physics are highly ionized systems, of H-like, He-like, and Li-like ions etc. He-like ions (atoms) are the simplest multi-electron systems, thanks to which they form a unique system that allows to test theoretical models demonstrating relativistic and correlative reciprocal influence of the electrons on the structure of atomic levels as well as on the dynamics of atomic processes such as ionization, excitation, capture or recombination. Therefore, over the past decades, intensive studies have been carried out on the formation of excited states in He-like ions and their decay. With the use of accelerators and ion traps, such studies were carried out on low and mid-Z ions. They covered electron capture to H-like systems, electron excitation in He-like systems and K-shell ionization of Li-like ions.

Attempts to find suitable experimental techniques allowing for high selectivity in the production of low-energy S and P states were an especially important part of the studies. High selectivity techniques in production of suitable atomic states greatly facilitate performing precise spectral analysis of strongly ionized atomic systems which, by nature, have multiple possible electron configurations. So far, selective production of atomic states has been observed only for Ar ions in plasmas produced by Electron Cyclotron Resonance Ion Source (ECRIS) type of ion sources [B1]. With systems of high atomic numbers and the use of ECRIS ion sources, such production is impossible.

The aim of my studies was to develop techniques for the production of S and P states in heavy He- and Be-like ions during relativistic ion-atom collisions in the target. The primary objective of the studies was to determine the degree of selectivity of S [1s2s] state production in He-like ions induced by K-shell ionization of Li-like ions in high-Z atoms (Ur-like ions, in this case). In order to meet this objective, I analysed the x-ray spectra collected during the experiment carried out in the storage ring at the GSI laboratory near Darmstadt, Germany. Apart from determination of the selectivity of S states production in Ur ions degree, I aimed to characterize their exotic decays resulting from magnetic M1 ([1s2s] $^3S_1 \rightarrow$[1s^2] 1^1S_0) and double-photon 2E1 ([1s^{1}2s^1] $2^1S_0 \rightarrow$[1s^2] 1^1S_0) transitions.

Through the analysis of angular decays as well as relative intensities of the above transitions, it became possible to test models that presented exotic atomic states formation, including the so-called statistical model, the sudden approximation or, ultimately, the first-order perturbation model. Presentation of high selectivity in terms of S [1s2s] states production in the above studies, enabled detailed investigation into: two-photon decay spectra of [1s^{1}2s^1] 2^1S_0 state, parity non-conservation and nuclear excitation mechanisms by two-photon transitions. The analysis of X-ray spectra recorded in coincidence with electron capture by U^{89+} was performed with two aims in mind. First, to obtain new information on the

formation of excited P-states in Be-like uranium ions (U^{88+}). Second, to demonstrate that the structure of these spectra related to radiative electron capture enables tests of radiative recombination theory and electron capture and may be used as a useful tool for Compton's profiles analysis of the low-Z atoms and molecular systems.

The next important objective of my studies on exotic atomic processes was to investigate interaction of a single photon with the atom's electrons, which may lead to the formation of hollow atoms, i.e. doubly ionized atoms in the K-shell. Studies into such atoms expand our knowledge of atomic processes on the femtosecond time scale. The hypothesis particularly analyzed concerned a dominant role of a quasi-classical knockout (ionization) resulting in double photoionization of low- and mid-Z K-shell atoms within the threshold energy range (double ionization). Moreover, the analysis was performed to use the x-ray lines broadening, observed in the decays of doubly-ionized states in the K-shell, as a signature of other processes that accompany double photoionization, including strong processes of electron shake-off from the valence shells.

In the studies there was also an attempt to reconstruct transitions of the most precise experimental two-electron x-ray transitions and their relative intensities (in relation to one-electron transitions). The attempt was based on a carefully designed model using multiconfiguration Dirac-Fock calculations, which controls for the so-called electron substitutions. The above studies enabled testing this type of calculations in case of hollow atoms, which are definitely one of the most exotic atomic systems.

The analysis of high-resolution x-ray spectra arising during stopping and in plasmas was a key aim of my studies. Heavy ions that bombard targets with energy exceeding 1 MeV per nucleon and mass over 20 A (A means the mass number) lose most of their energy during stopping, as a result of ion-target interactions. Energy density deposited within the atom (1nm diameter) during stopping (within 10^{-17}s) can be very high, of about 50-70 keV per nm. Such a large energy transfer from an excited atomic system to a crystal lattice may cause structural and phase transformations alongside ion beam trajectory at the nanometre scale [B2].

Detailed knowledge of primary electron states excited by strong coulomb fields coming from the ions that penetrate the target is required to describe a ion beam trajectory formation. Strong dependence of the probability of shell excitation and ionization on the collision parameter during ion-atom reaction may lead to the formation of non-equilibrium charge distribution in the atoms of the target.

Therefore, one of the basic aims of my studies in the field was to develop understanding of unique features of non-equilibrium electron states relaxation. The phenomenon determines time and space evolution of the energy deposited upon stopping, and thus subsequent distributions of electron temperature and density of the so-called plasma microstructures which may form around the penetration path in the solid target.

Ion-atom interactions, occurring when collision parameters are high, cause outer-shell ionization, whereas central collisions (when collision parameters are low) are responsible mainly for inner-shell ionization, which often causes emission of specific x-ray radiation by the ion as well as the atoms of the target. Analysis of high-resolution x-ray spectra arising during ion stopping in matter provides unique information on electron structure of individual stopping media during subsequent phases of stopping within the first few femtoseconds since ion-atom interaction. This knowledge is key for many potential applications related to ion stopping: from radiative damages, material nano-modifications, plasma microstructures generation up to the use of heavy ion beams in oncological radiotherapy [B3], [B4], [B5], [B6].

In contrast to many others, high-resolution x-ray diagnostics provides valuable information on stopping dynamics. In particular, X-ray radiation registered in high spectral resolution is a signature feature of a given charge state of an ion penetrating the target. Owing

to this, it enables direct analysis of stopping of the ions of a given charge state (other diagnostics allow only to obtain averaged information of all charge states). As a result, determination of the evolution of radiation emission for different depths of ion penetration of the target became an important aim of the conducted x-ray measurements of spatial resolution alongside the stopping track of the ion beam. Special significance of high-resolution x-ray diagnostics in the studies of the ion stopping in matter processes is also confirmed by the fact that K-series x-ray measurements accompany the ion-atom interaction with low impact parameters in collision at the atomic scale, and thus allow to obtain experimental data for a well-defined range of impact parameters. Such data are very useful in testing the theories of ion energy loss in solids.

The analysis of X-ray spectra arising in high-temperature plasmas is the next study area presented in this summary. Such studies are of immense relevance as well to the development of theoretical atomic models as to the applied studies, especially those concerned with the issue of nuclear fusion. X-ray radiation emitted from plasma by highly ionized high-Z ions conveys unique information about relativistic quantum-electrodynamic (QED) and about their correlations, the so-called virtual electron correlations in particular. Ne- and Ni-like ions are also considered as potential x-ray laser sources [B7].

In nuclear fusion studies, analysis of x-ray spectra of mid- and high-Z atoms allows to obtain key plasma parameters, such as the level of metallic impurities, ion and electron temperature, rotational velocity and Z_{eff} (effective plasma charge) [B8]. The necessity of detailed spectroscopic studies of tungsten was triggered by the choice of this element for the surface material of the latest International Thermonuclear Experimental Reactor (ITER). This also led to launching the European research programme in the largest tokamak in Europe - Joint European Torus (JET) based in Culham, (Great Britain). The programme aims to investigate selected plasma scenarios for ITER. A high-resolution x-ray spectrometer was used in the programme as one of the most important diagnostic tools. My participation area in the programme covered a range of issues related to high-resolution x-ray diagnostics in JET laboratory. These issues ranged from designing modifications of the existing diagnostics, through the construction of gas x-ray detectors and their energy and efficiency calibration up to the advanced theoretical calculations of suitable spectral lines necessary for accurate interpretation of the measured x-ray spectra. Ensuring possibility to monitor soft x-ray radiation (2-12 keV) emitted by Ni^{26+}, Mo^{32+} as well as W^{45+} and W^{46+} ions from the central plasma area of JET tokamak was the main purpose behind the modification of high-resolution x-ray diagnostics. These studies expand the current knowledge about the influence of metallic impurities on key parameters of the plasma generated in thermonuclear reactors.

The last study area presented in this summary is making a design of the conditions for registering nuclear excitation by electron capture (NEEC) to an unfilled electron shell of the atom. Nuclear isomers, i.e. long-lived, metastable states of nuclei [B9] may store massive amounts of energy, even million times greater (per mass unit) than the latest chemical batteries. Already in 1976, Goldanskii and Namiot [B10] noticed that the possibility to trace NEEC, i.e., the reverse process of the well-known internal conversion (IC) [B11], would be of fundamental significance for nuclear physics and application studies. In 1989, Cue, Poizat, and Remillieux put forward the list of isotopes suitable for experimental observation of NEEC due to their metastable states [B12]. In 2007, Palffy et al. [B13] presented predictions of active sections for NEEC for the isomers of several elements. While in 2012, Karamian and Carroll [B14] conducted qualitative research into the possibility of NEEC for ^{93m}Mo isomer.

The pioneer character of the issues as well as 40 year long difficulties in observing NEEC inspired me towards the studies whose main aim was to determine optimal conditions for tracing and gaining detailed understanding of NEEC for nuclear isomers of several elements. A particularly interesting and important case of ^{93m}Mo ($T_{1/2} \sim 6.8$ h) nuclear isomer

was the subject of the first part of the studies, which was conducted in close cooperation with J. J. Carroll's group (the USA) and Prof. M. Polasik's team from the UMK in Toruń. Detailed studies using various methods of atomic and nuclear physics were carried out due to the multitude of factors that had to be considered while designing the experiment. Our unique experimental configuration included three key elements: the use of Gammasphere spectrometer, optimal target construction, and right amount of energy of ^{90}Zr ion beam. Acting in concert, they enabled us eventually **to observe NEEC for the first time for ^{93m}Mo isomer [A11], i.e. to identify a new** physical phenomenon. It is also worth emphasizing that within the framework of recently planned new experiments with the use of ^{93m}Mo and ^{242m}Am isomers, I am going to continue pursuing the subject of NEEC to gain higher degree of expertise in these processes.

It is noteworthy that obtaining detailed knowledge and understanding of NEEC processes may greatly influence development of the theories on the structure, formation and evolution of high-spin states of nuclei. Obtained knowledge will facilitate understanding of the processes that occur in the Universe, and, in particular, will provide us with the most important information regarding living of the various elements isotopes' nuclei in stars' environment. The mentioned knowledge could also serve as a starting point for applied studies, whose aim would be to enable controlled energy release stored in nuclei isomers of given elements. Finding out about the nature of NEEC process should promote development of new, unconventional, ultra-efficient nuclear batteries which could be used for powering vehicles (ships) in hardly accessible places on the Earth (at the bottom of oceans and volcanic craters) and in space.

4.3. Discussion of the results

4.3.1. Study of the selectivity in the production of S and P states in He- and Be-like ions during ion-atom collisions.

My studies on the production of S and P states in He- and Be-like ions during relativistic ion-atom in the target collisions were conducted on the basis of the data collected in the experiment done in GSI laboratory in Darmstadt. Uranium ions accelerated in an ISIS synchrotron to the energy of 98 and 398 MeV/A (A is the ion mass number) were used in the experiment. Subsequently, the ions were injected into the storage ring in the proper charge state (Li –like U^{89+} ions) and number (about 10^8 ions). Li-like uranium ions were collided with the gas jet of molecular nitrogen (N$_2$) target. X-ray spectra accompanying ion-atom collisions were recorded in coincidence with selected charge states with Ge detectors set around the jet target. Schematic experimental system built around the area of ion beam interaction with the gas target in the storage ring is presented in Figure 1.

X-ray spectra analysis was performed in coincidence with selected U^{90+} (He-like ions) and U^{88+} (Be-like ions) charge states formed respectively during ionization and electron capture resulting from the collision of U^{89+}ions with the atoms of the target. X-ray spectra accompanying U^{89+} (98 MeV/A)$\rightarrow$N$_2$ collisions for different coincidental conditions are presented in Figure 2. The structure of observed x-ray spectra in coincidence with ionization [Figure 2 (d)] and theoretical analysis of the dependence of probability of ionization for different parameters of the collision indicated that K-shell ionization of Li-like uranium ions during relativistic collisions with light gas targets is highly selective and leads to the population of almost only 2^1S_0 and 2^3S_1 states in He-like systems. It was indicated that P states impurities by the exotic process of simultaneous ionization and electron excitation $2s_{1/2}\rightarrow2p_{1/2}$ or $2s_{1/2}\rightarrow2p_{3/2}$ do not exceed 0.05% [A1]. In other words, a passive role of $2s_{1/2}$ electrons during K-shell ionization of Li-like uranium ions in relativistic collisions with light gas targets was demonstrated.
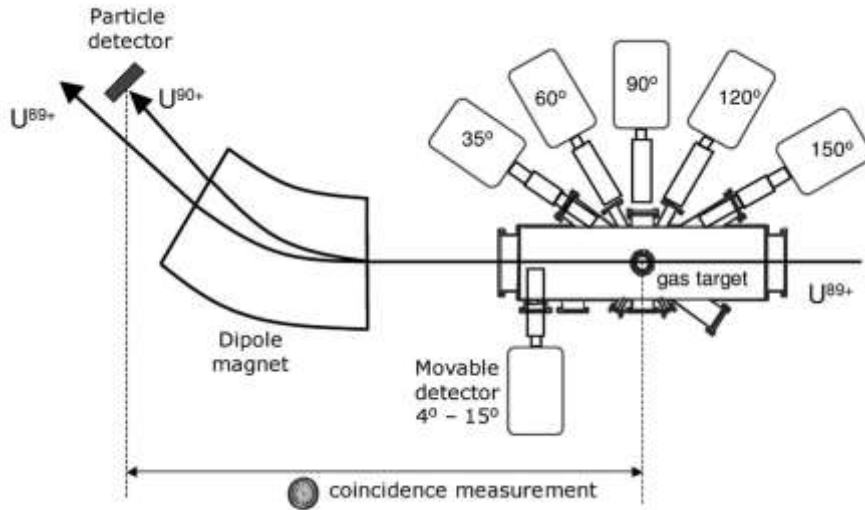
Figure 1. The experimental system set-up around the area of uranium ions interaction with the gas target in the storage ring in GSI Darmstadt laboratory for the measurements of x-ray spectra accompanying relativistic interactions $U^{89+} \rightarrow N_2$ [A1].
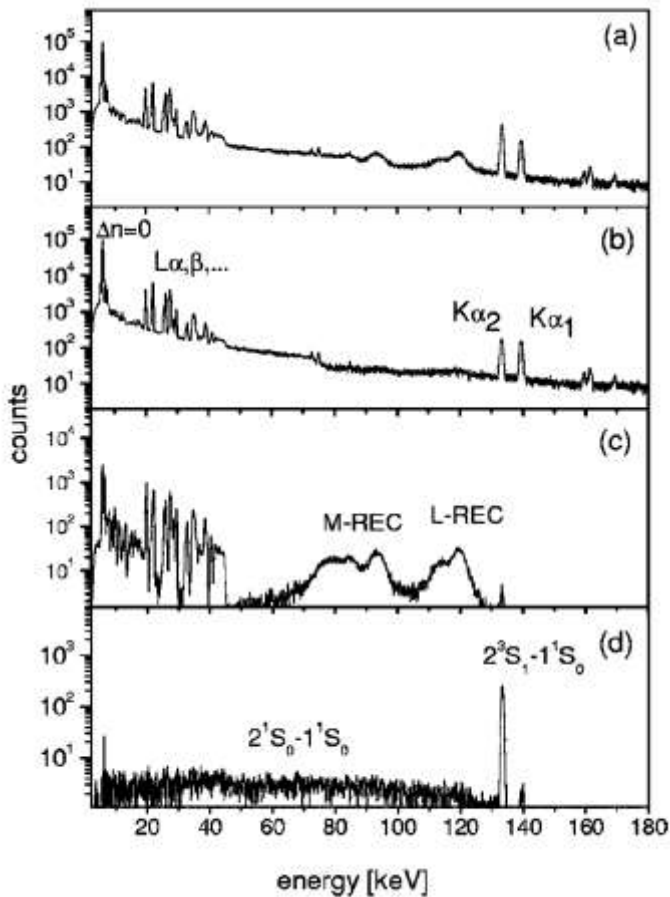

Figure 2. X-ray spectra recorded in U^{89+}(98 MeV/A)$\rightarrow N_2$ collisions at 35° angle to ion beam axis direction, (a) total spectrum recorded without coincidence, (b) spectrum recorded in the so-called anticoincidence with the charge exchange corresponding to Li-like U^{89+} ions' excitations, (c) spectrum recorded in the coincidence with electron capture, spectrum corresponding to U^{88+} Be-like ions, and (d) spectrum recorded in coincidence with ionization corresponding to U^{90+} He-like ions [A1].

The analysis of relative intensities of x-ray transitions that correspond with de-excitation of the following states: 2^1S_0 (2E1 two-photon transitions observed in the spectrum

as a continuous structure) and 2^3S_1 (M1 magnetic transition) enabled defining relative probabilities of S states formation due to K-shell Li-like uranium ionization during relativistic collisions with light gas targets. Formation of 2^1S_0 and 2^3S_1 states occurs in two consecutive steps. In the first, ionization takes place, whereas in the second, an electron coupling with the states of a given angular momentum. In the description of the sudden approximation model, probability of He-like S state formation as a result of ionization depends only on the initial wave 2s electron function in the Li-like ion coinciding with the final wave function for He-like configurations, 2^1S_0 and 2^3S_1, respectively. An uranium ion whose energy is about 100 MeV per nucleon or higher is considered as a highly relativistic system. In such a case, spatial distribution of 2^1S_0 and 2^3S_1 orbitals should not depend on electron coupling. Therefore, in accordance with the sudden approximation model, probability of 2^1S_0 and 2^3S_1 states ratio should equal [1s2s] $^1S_0$ / [1s2s] $^3S_1 \approx 1$.

The analysis of relative experimental intensities of x-ray transitions demonstrated coincidence with the predictions of the sudden approximation model only in highest energy uranium ions (398 MeV/u which equals 71% of the speed light and exceeds the K-shell electron speed in uranium ions) colliding with the atoms of the gas target I(2E1)/(M1)=0.97±0.08. In case of lower energies (98 MeV/u, which equals 43 % of the speed light and does not exceed the electrons speed of the in the K-shell in uranium ions) the result of relative intensities was significantly lower I(2E1)/(M1)=0.64±0.06, which explicitly indicates a breakdown of the sudden approximation model [A1]. It is also worth mentioning that the obtained results are not consistent with the so-called statistical model which should scale as *2J+1* (*J* – the total angular momentum). According to the mentioned statistical model, the formation probability ratio of states 2^1S_0 and 2^3S_1 should equal [1s2s] $^1S_0$ / [1s2s] $^3S_1 \approx$ ⅓. Moreover, angular distribution analyses demonstrated anisotropy of x-ray radiation that accompanies two-photon transitions 2E1 with the enhanced radiation in parallel direction to the beam (Figure 3). Also, new experimental information on excited states $[1s^2 2s2p_{3/2}]$ $^1P_1$ and $[1s^2 2s2p_{3/2}]$ $^3P_2$ formation in Be-like uranium ions was obtained thanks to additional x-ray spectra analysis in coincidence with electron capture [Figure 2(c)]. It was indicated that in contrast to K-shell ionization which leads to non-statistical S states formation in He-like ions, electron capture processes lead to $^1P_1$ and $^3P_2$ states formation in accordance with *2J+1* statistical distribution.

Rich spectra structures connected with Radiative Electron Capture (REC) to L, M up to Q shells (n=7) were observed in x-ray spectra recorded in coincidence with the electron capture to U^{88+} ions (U^{89+} before the capture). This enabled testing the theoretical cross sections for radiative recombination under the conditions of highly non-symmetrical relativistic collisions ion-atom. The possibility of testing processes connected with cascades of radiative x-ray transitions from high electron states (at least to n=7 states) taking account virtually of all kinds of electric and magnetic (E1, M1, E2 and M2) transitions. Finally, it was suggested to use the above x-ray spectra as a useful tool for performing Compton's profiles analysis of light atomic and molecular targets [A3].

It should be emphasized that the most important result presented in this part of the summary concerned the determination of high selectivity of [1s2s] $^1S_0$ states production in He-like uranium ions arising due to K-shell ionization of Li-like ions. The result has in fact occurred to be a new tool for studies on decays of two-photon [1s2s] $^1S_0$ states in He-like ions. As regards x-ray spectra recorded in coincidence with electron capture, it has been proven that their structure which relates to radiative electron capture not only allows for rigorous tests of theoretical models but can be also a practical tool for Compton's profiles' analysis.
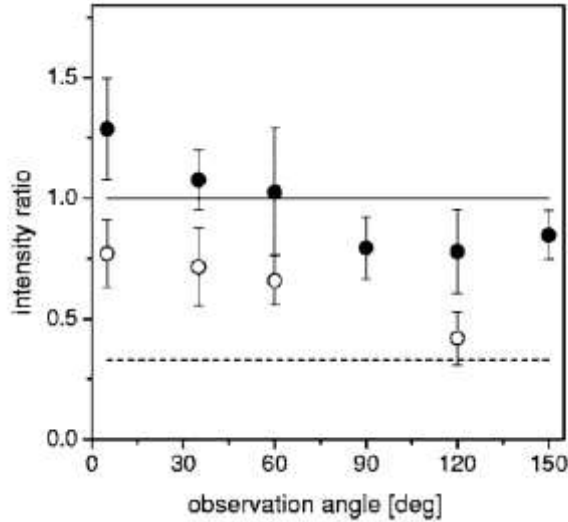
Figure 3. Intensities ratios of 2E1/M1 transitions in U^{90+} uranium ions as a function of the observed angle for U^{89+} ions collisions with N_2 (open points measured for 98 MeV/A energy; black points for 398 MeV/A energy). The solid line represents the prediction of the sudden approximation model, the dash line represents the prediction of statistical population of [1s2s] $^1S_0$ and [1s2s] $^3S_1$ in He-like uranium ions [A1].

The results of this part of the studies have been published in two articles ([A1] and [A3]) in journal from the ISI Master Journal List.

4.3.2. Study of the interaction of a single photon with the electrons of an atom leading to the creation of doubly-ionized atoms in the K-shell

K-shell hollow atoms, i.e. doubly-ionized atoms in the K-shell (K^{-2}) constitute an attractive environment for studying the nature of exotic atomic states and mechanisms leading to their production. Such atomic states can arise as a result of several different physical processes, including nuclear decays and ion-atom collisions. Double photoionization is a highly interesting process which can result in the arising of K-shell hollow atoms. A single photon absorption in this process is followed by a purely quantum process of electron shake-off (SO) or a semi-classical process of a knockout (ionization) of the second electron from the K-shell.
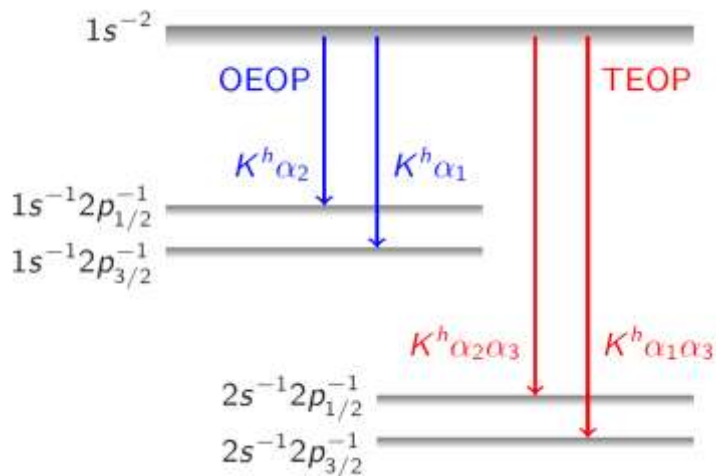

Figure 4. The diagram of one- (OEOP) and two-electron (TEOP) x-ray transitions that accompany de-excitation of doubly-ionized atomic states in the K-shell [A9].

11

Doubly-ionized atomic states in the K-shell are the atomic states of the shortest life times (below 1fs). They decay *via* nonradiative *Auger* transitions or *via* one-electron one-photon (OEOP) or, significantly weaker, two-electron one-photon (TEOP) radiative transitions. Figure 4 shows the diagram of possible decays of radiative atomic states doubly ionized in the K shell. One-electron transitions in hollow atoms in the K-shell are called hypersatellite $K^h\alpha_1$ and $K^h\alpha_2$ transitions. Hypersatellite $K^h\alpha_1$ and $K^h\alpha_2$ lines widths observed in x-ray spectra carry direct information on life times of doubly ionized atomic states in the K-shell. Recent high-resolution measurements of the widths of hypersatellite lines obtained due to double photo-ionization demonstrated that experimental values are clearly higher than the most accurate theoretical estimates.

Despite many attempts to estimate fluorescence yields of K^{-2} states more precisely, discrepancies between the theory and the experiment were not explained. All these considerations led to the hypothesis that cast doubt on the theoretical estimates on the widths of hypersatellite lines and, consequently, to the necessity to put forward a new theory of the K^{-2} states arising [B15].

An innovative approach to the issue of the analysis of hypersatellite $K^h\alpha$ x-ray spectra measured for solid targets was presented within the framework of my studies. In the first step, radiative natural widths of K^{-2} states with Multi-Configuration Dirac-Fock's (MCDF) calculation which involves Breit interaction and QED effects. However, so marked widths of hypersatellite lines were significantly lower than those observed experimentally.

Therefore, in the next step, Open-Shell Valence Configuration effect (OVC) had to be included in x-ray spectra simulations. The effect stems from the fact that in case of open-shell atoms, there may be indicated many initial K^{-2} and final $K^{-1}L^{-1}$ states for each kind of a hypersatellite transition. A transition, but actually, a given group of transitions consists then of numerous, over-lapping components of diverse energies and widths. The OVC effect, as a consequence, causes the increase of effective widths of $K^h\alpha_1$ and $K^h\alpha_2$ natural lines. Atomic valence configurations in solid states differ from such configurations in free atoms. Therefore, in the widths of hypersatellite lines simulations that include the OVC effect, a linear combination of valence states was adopted in order to approximate averaged valence configurations foreseen by advance valence spectrum calculations to the highest possible extent. Figure 5 shows the broadening of $K^h\alpha_1$ and $K^h\alpha_2$ lines due to the OVC effect. Including the OVC effect in case of open-shell atoms allows to decrease the discrepancies between the theoretical and experimental widths of hypersatellite lines [A5].

Another reason for a significant broadening observed in $K^h\alpha$ X-ray lines widths measurements lies in the effect of outer-shell ionization and excitation (OIE). The estimation of the OIE factors which contributed to the hypersatellite $K^h\alpha$ lines broadening required not only theoretical calculations of the electron shake-off (SO) probabilities but also proposing various characterization of electron shake-off processes from outer atom shells for different ranges of photon energies.

The first proposed scenario (OIE1) concerned a photon-electrons interaction within the range of high-energy (photon energy levels which are significantly higher than the energy level of K electrons binding in an atom). Photoionization that occurs during the process (due to a photon absorption by a single electron from the K-shell) causes instant, and high-velocity knockout of the primary K-electron. The second K-electron ejection (shake-off) may result from the sudden approximation. In contrast to the first one, the second electron is ejected with considerably lower velocity. Consequently, the valence electron shake-off process is relatively weak as valence electrons are impacted only by the sudden approximation that comes from singular ionization of the K-shell. Theoretical considerations led to the fact that the OIE1 scenario was considered as stemming from the double-ionization mechanism within high energy levels area caused by the purely quantum process of electron shake-off (SO). A

slight narrowing of the specific widths of hyper-satellite lines in a consequence of this process, observed in x-ray spectra.
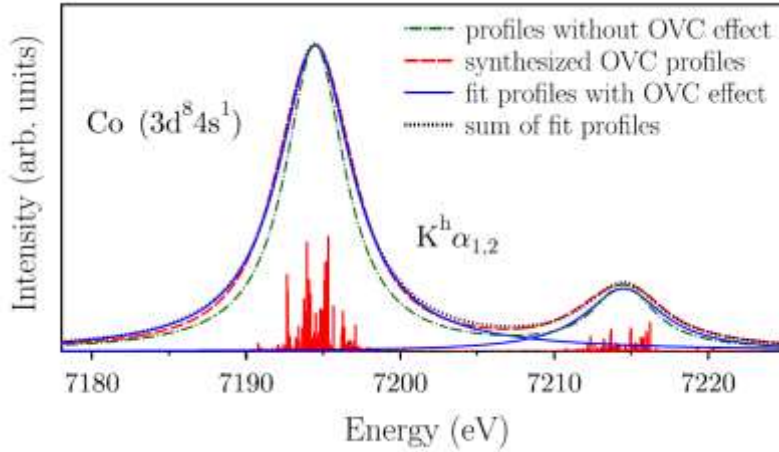

Figure 5. The theoretical simulations of $K^h\alpha_1$ and $K^h\alpha_2$ x-ray transitions in Co-atom, including the OVC effect [A5].
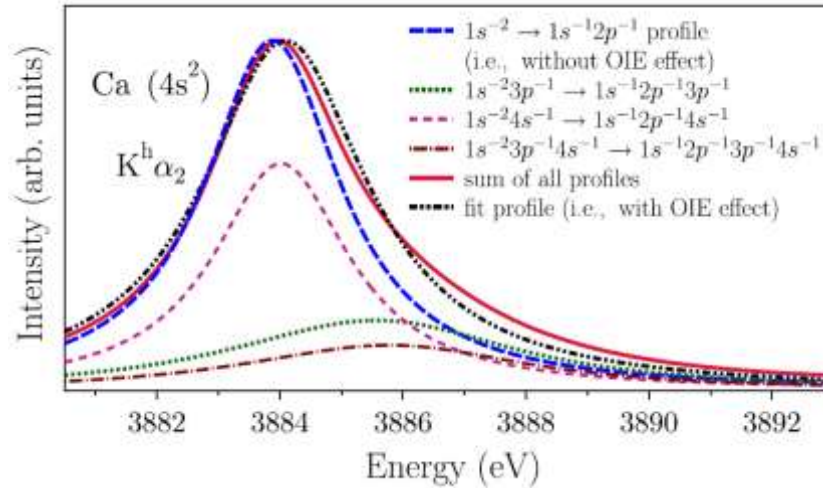

Figure 6. The theoretical simulations of $K^h\alpha_2$ x-ray transitions in Ca-atom, with the effect of ionization and electron excitation in outer atomic shells (OIE2) [A5].

The second proposed theoretical model characterizes double photoionization within the range of medium and low photon energies. In this case, the primary K-electron ionization precedes the semi-classical process of the second electron knockout (ionization) from the same shell. This means that at the same time both K-electrons are ejected from the atom. In contrast to the OIE1 process, impact on valence electrons caused by the sudden approximation is much stronger in OIE2. Accordingly, there is a multiple increase in the probabilities of the outer-shell electrons shake-off. For instance, for 3d valence shell in Ca-atom this probability increases from about 15% to almost 46%. Strong outer-shell electron shake-off cause additional broadening of hypersatellite lines observed in the x-ray spectra of hollow K-shell atoms. Figure 6 shows $K^h\alpha_1$ and $K^h\alpha_2$ lines broadening due to OIE2 effect.

Reconstruction of the broadening of hypersatellite $K^h\alpha_1$ and $K^h\alpha_2$ lines observed in the measurements of x-ray spectra induced by low and mid energy level photons is possible only when both effects, OIE2 and OVC for open shell atoms, are taken into account. Therefore, a predominant mechanism responsible for double photoionization of the K-shell within the range of low and mid energy of the photons that interact with atom electrons is a semi-classical process of the second electron knockout from the K shell. In addition, this semi-classical process causes a strong shake-off of the electrons from the outer shell. It is also worth emphasizing that low and mid photon energy range corresponds to the maximum cross

13

section for double (photo)ionization. For this reason, it is really important to explain hypersatellite lines broadening in the mentioned photon energy range. Moreover, since a hypersatellite line broadening depends on the type of K-shell double photoionization, the presented analyses provided a new tool in determining the relative role of double ionization mechanisms in different energy ranges of photons interacting with atom electrons.

The next part of my research into hollow atoms in the K-shell conducted within last years aimed at determining characteristics of TEOP transitions through which such atoms can de-excite. The possibility of two-photon de-excitations was first foreseen by Heisenberg in 1925 [B16]. In 1931, Goudsmit and Gropper [B17] formulated proper selection rules for TEOP transitions, and in 1973 Wölfli [B18] et al. published for the first time a research paper on the experimental observation of TEOP transitions in Fe and Ni atoms. Since then TEOP transitions have been the subject of intensive theoretical and experimental studies.

In recent years, Hoszowska et al. [B19] carried out an exceptionally precise synchrotron experiment. They measured energy levels, relative intensities (towards one-electron transitions), and widths of the lines which corresponded with two-electron transitions (TEOP) in doubly-ionized in the K-shell Mg-, Al-, and Si-atoms. The obtained experimental data enable the most rigorous tests of theoretical calculations that characterize exotic atomic states. The comparison of theoretical and experimental values demonstrated a good agreement only for TEOP transition energies. Two-electron transition relative intensities and corresponding x-ray spectra widths were not well reconstructed by past theoretical models. Relative intensities of two-electron transitions, obtained on the basis of two theories: the second-order perturbation theory using hydrogenlike wave functions and the Hartree-Fock and Dirac-Fock (MCDF) theory underestimate experimental values by factor of 2-3. Only an advanced theory that takes into account the so-called virtual relativistic configuration interaction (RCI) allows to reduce discrepancies between the experiment and the theory to the level of 15-30%.

In my studies on two-electron transitions, I made an attempt to reconstruct the experiments carried out by Hoszowska et al. and assess relative intensities of TEOP transitions in Mg-, Al- and Si-atoms. Hoszowska et al. obtained impressively precise experimental values as regards exotic atomic states in general, i.e. with 14% and 19% error [B19]. Theoretical energy levels and TEOP transitions' intensities were determined with MCDF calculations that involves Breit interaction and QED effects. Additionally, the calculations were expanded by the effects of relativistic configuration interaction (MCDF-RCI). Relative intensities of TEOP transitions were calculated as well in the so-called transverse gauge (Coulomb's) as in the length gauge (Babushkin's). The difference between the rates in two gauges is a typical method to test quality of the calculations in consecutive developments of the RCI method. Calculations were made for both single and double substitutions. It was indicated that including double substitution allows to reduce the TEOP rates ratio, calculated in the length and transverse gauge, to the value nearly equal to 1, which confirms good quality of the theoretical results.

Similarly as in case of OEOP transitions, a further step towards an advanced theoretical model on two-electron transitions was the incorporation of the OVC effect and outer K-shell electron ionization and excitation due to powerful potential change related to the double K-shell ionization (OIE1 and OIE2). Out of all past theoretical calculations in reconstruction of experimental values, TEOP/OEOP rates, including virtual electron states correlations and strong ionization and electron excitations in the outer shells (OIE2) have been the most accurate [A9]. This is presented in Figure 7.

In the next step, an attempt was made to theoretically reconstruct experimental values of TEOP lines' widths ($K\alpha\alpha^h$). As an x-ray line width corresponds to the sum of the widths of initial and final states, calculations of radiative and nonradiative K^{-2} states (the group of initial

states) and L_1^{-1} $L_{2,3}^{-1}$ (the final states group) were made to determine the theoretical values of $K\alpha\alpha^h$ line. It is worth to emphasize here that according to the best of my knowledge, the calculations described above have never been published before. Further improvement of the obtained theoretical values required including corrections related to the open valence shell (OVC) and strong ionization and excitation of outer atom shell electrons (OIE2), 3s and 3p shells in particular. Contributing factors of both effects to the broadening of x-ray lines corresponding to two-electron transitions in Si-atom are presented in Figure 8.
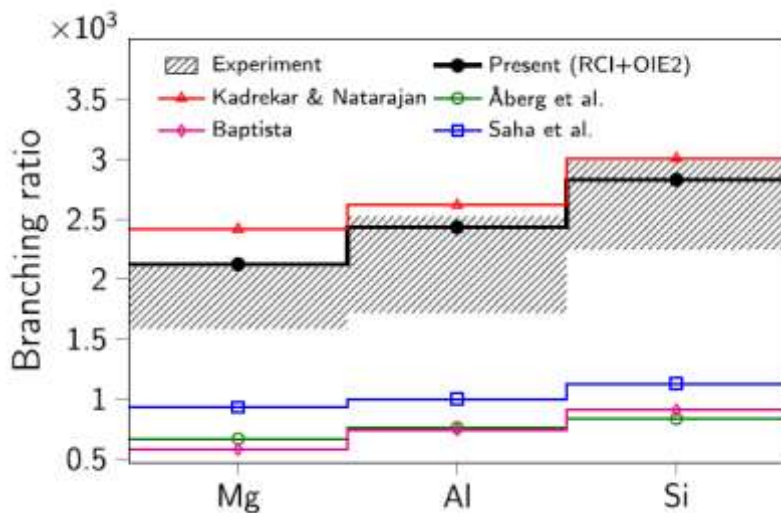

Figure 7. The comparison of theoretical and experimental TEOP/OEOP rates [A9].
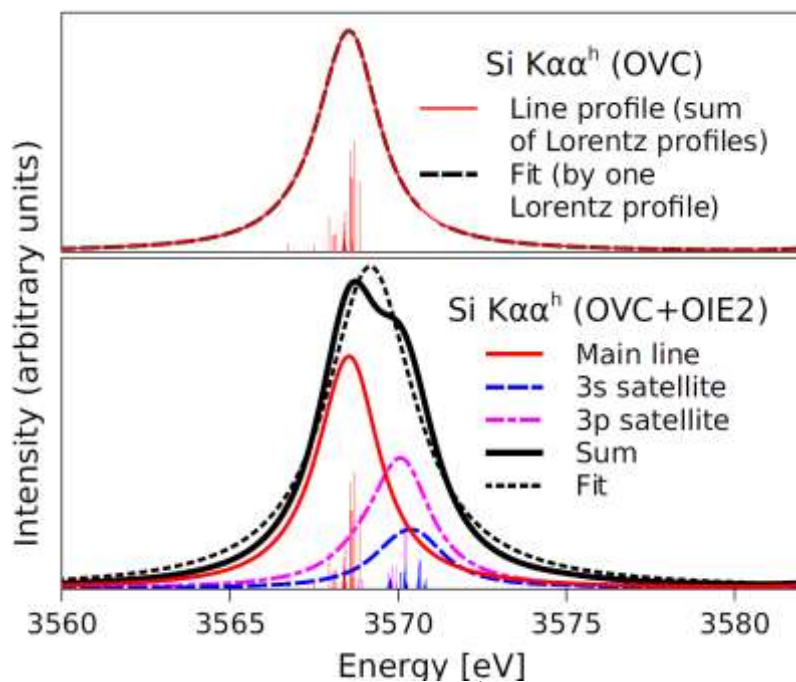

Figure 8. Theoretical simulations of $K\alpha\alpha^h$ x-ray transitions in Si-atom including the OVC effect (upper Figure) and the OVC effect with the effect of strong ionization and electron excitation in the 3s and 3p shells OIE2 (lower Figure) [A9].

Summing up this part of the presented studies, it should be stated that it is possible to reconstruct experimental widths of natural x-ray lines that correspond to OEOP and TEOP transitions and their relative intensities for low-Z atoms. In order to make such a reconstruction, one should use advanced MCDF-RCI calculation models that include the open shell effect together with the effect of strong ionization and excitation of the electrons in the

15

outer atom shells. The obtained theoretical values correspond closely to the experimental ones. The results of these studies set new limits for theoretical calculations on one- and two-electron transitions for hollow atoms in the K shell of low Z value.

The results of this part of the studies have been published in two articles ([A5] and [A9] in the prestigious journal *Physical Review Letters* and *Physical Review A* (as Rapid Communication) from the ISI Master Journal List.

4.3.3. The analysis of high-resolution x-ray spectra arising during ion stopping in solid targets

The studies of high-resolution x-ray spectra accompanying subsequent phases of calcium ions stopping in silicic targets were conducted on the linear accelerator UNILAC in GSI institute in Darmstadt (Germany). Ca-ions in the initial charge q=+6 state and initial energy of 11.4 MeV/A were entirely stopped in solid SiO_2 targets of lowered density (~0.023 g/cm3) and 25-mm thickness. Due to an innovative technology of diluted silica production in the form of low-density aerogel, specially designed targets were prepared. They were to enable measurements of characteristic x-ray radiation for different ion penetration depths in the target. Owing to aerogel silicic targets it was possible to increase the stopping length of ions of energy level 11,4 MeV/A from ~100 μm (in typical silica) to 10 mm (in an aerogel target). In addition, aerogel targets significantly reduce x-ray radiation absorption emitted by the target, which makes it possible to observe the radiation emitted from direct ion-atom interaction area.
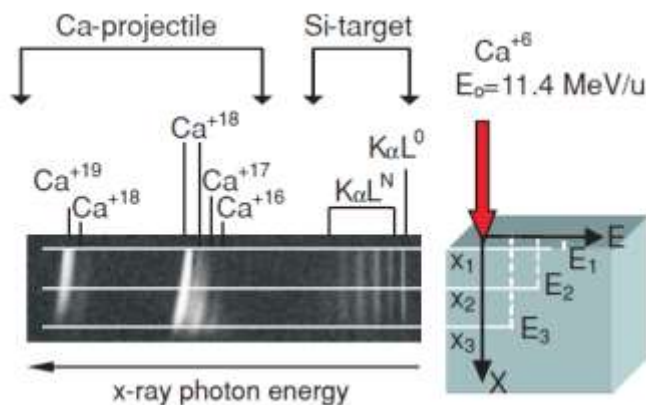
Figure 9. The x-ray image that shows the characteristic radiation of Ca-ions and Si-atoms of the target, registered in spatial resolution alongside the stopping path of the ions in the target (on the left). The diagram of high-resolution measurements of characteristic x-ray radiation arising during the stopping of Ca-ions in the aerogel SiO_2 target of low density (on the right). The (x) symbol represents the depth of ions penetration in the target, whereas (E) represents the average energy level of ions in a given phase of stopping dynamics [A4].

Characteristic K-series x-ray radiation emitted by the ions and target was registered with a diffraction spectrometer equipped with a spherically bent mica crystal (in the second and fourth diffraction order). The spectra were recorded in high-energy ($\Delta E \sim 0.4$ eV) and spatial ($\Delta x \sim$ several dozen μm) resolution. X-ray spectra of the radiation characteristic to Ca ions of charge states from q=+16 to q=+19 and Si atoms of the target registerd in spatial resolution alongside the stopping path in the target and the scheme of the measurements are shown in Figure 9. Doppler shifts induced by the ions whose energy levels

decrease with ions penetration depth, which are seen in the figure, were used for an exact determination of the ions' velocity in different stopping phases.
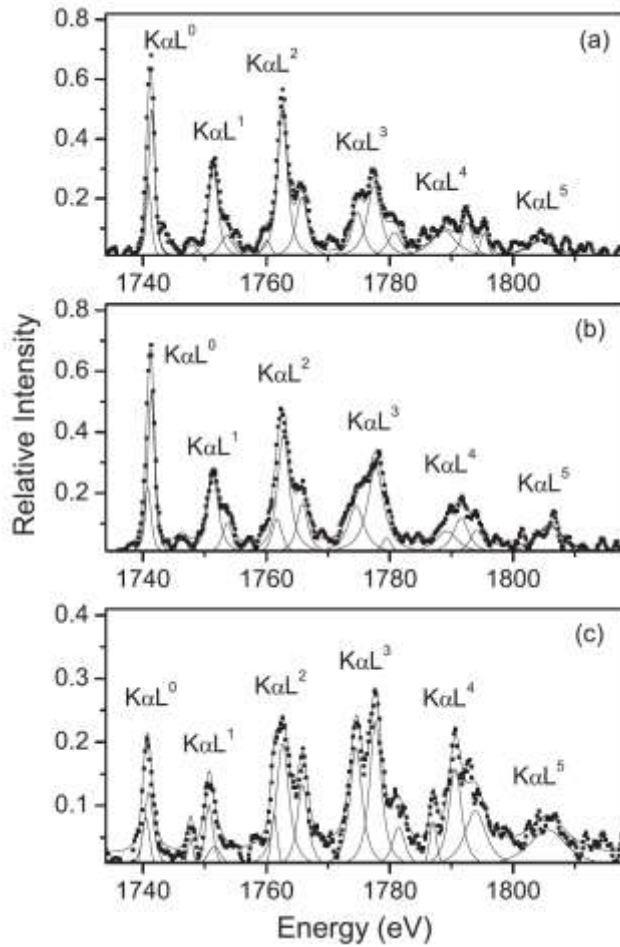

Figure 10. High-resolution K-series x-ray spectra induced in SiO_2 low-density aerogel target by Ca ions of different energy levels for different depth penetrations in the target; (a) ~0.5 mm (11.4–10.6 MeV/u), (b) ~5 mm (8.5–7.6 MeV/u), and (c) ~10 mm (5.2–4.0 MeV/u) [A4].

K-series x-ray spectra emitted by SiO_2 stopping medium contain the following components: diagram lines ($K\alpha L^0$) corresponding to electron transitions $2p\rightarrow1s$ in a single ionized Si atom in the K shell and the so-called satellite lines ($K\alpha L^N$) corresponding to electron transitions $2p\rightarrow1s$ in a single ionized Si atom in the K shell with additional N holes in the L shell. Due to a reduced screening of the charge of the nuclei, energy level shifts of $K\alpha L^N$ satellite are higher than the levels of $K\alpha L^N$ diagram ones. Satellite transitions energy level shifts depend on the number of holes in the L-shell. In the observed spectrum it is possible to resolve between individual $K\alpha L^N$ satellite lines (N=1, 2,…) corresponding to x-ray transitions $2p\rightarrow1s$ in the presence of an additional one, two etc., holes in the L shell due to significant energy shifts (higher than a natural x-ray line width).

With the use of an x-ray scanning procedure K-series spectra were obtained. The spectra were induced by Ca ions in the SiO_2 aerogel target and measured for three different penetration depths in the target (Figure 10). Well separated subsequent satellite $K\alpha L^N$ structures for consecutive ionization states in the L shell (N=1, 2,…) can be clearly seen in the spectra. Energy shifts corresponding to satellite lines in the M-shell (for consecutive ionization states in the M-shell) are significantly smaller than those originating from L-shell ionization. $K\alpha L^N$ lines, corresponding to x-ray transitions in the presence of additional holes in the M-shell, are broadened and shifted towards higher energies. Broadening and energy shifts depend on the level of M-shell ionization (the higher number of holes in the M-shell,

17

the higher broadening and shifts). Information on M-shell ionization (the ionization of the valence shell) is of key significance for the diagnostics of stopping dynamics of ions in solids, including diagnostics of nano-plasma structures formed around the ion trajectory in stopping medium.
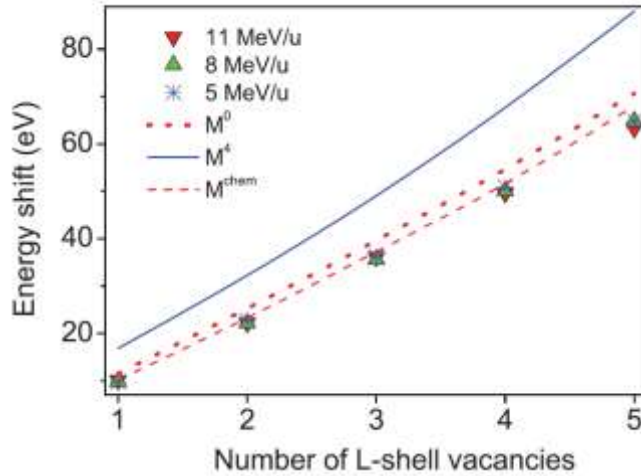

Figure 11. Comparison of experimental energy shifts of Si $K\alpha L^N$ lines measured for three different Ca energy levels (~11 MeV/A, ~8 MeV/A and ~5 MeV/A) including MCDF calculations for different configurations of the valence shell (M^0 neutral atoms $3s^2 3p^2$ valence configuration, M^4 highly ionized valence configuration, M^{chem} valence configuration enriched with oxygen electrons) [A4].

An advanced data analysis was performed for an accurate interpretation of K-series spectra induced by Ca ions in the aerogel SiO_2 target. The analysis covered matching corresponding spectra structures (peaks) including natural and instrumental broadening as well as advanced theoretical calculations (MCDF, ionization dynamics, electron capture and electron rearrangement in a time between the ionization and characteristic x-ray radiation). Due to the fact that x-ray spectra emitted from the stopping medium come from the SiO_2 compound (not from homogeneous silica), chemical effect had to be included in the analysis. Therefore, in the analysis the rearrangement of valence oxygen electrons towards valence structures of silica atoms (highly ionized in the inner atom shells) in a time between ionization and radiation was taken into account.

Thanks to these analyses, it was possible to determine precise experimental data on the intensity and energy of $K\alpha L^N$ x-ray radiation emitted by silica atoms (SiO_2) in three different phases of Ca ions stopping. The analyses also showed reduction of energy shifts of $K\alpha L^N$ satellite lines with respect to diagram lines $K\alpha L^0$ in x-ray spectra measured in all phases of Ca ions stopping under consideration. Observed in the experiment, energy $K\alpha L^N$ shift reductions, origin from chemical electron enrichment of the valence structure of highly ionized silica atoms [A4]. Furthermore, it was indicated that the strength of this effect increases with the ionization of silica atom in which transition $K\alpha L^N$ occurs (Figure 11).

Last part of the above analyses concerned the possibility of forming nano-plasma structures around the Ca ion trajectory which occurs during ion stopping in the target. Lankin et al.'s hypothesis on this possibility [B20] posited that low-temperature nano-plasma structures are formed due to ion-atom interaction. Such interaction should lead to the production of a large number of the so-called secondary electrons which, in turn, may ionize nearby atoms around the ion track. The model is based on the assumption that nano-plasma structures are localized within the ion track core with electron temperature of 10-50 eV and density 10^{23} cm^{-3}.

Such conditions (corresponding to the plasma effective charge $Z_{eff}>6$) would have to lead to the entire ionization of the M-shell. This part of the hypothesis is clearly contradictory to the results of the x-ray spectra analysis presented above, according to which the M-shell is not ionized, but, to the contrary, enriched with additional valence electrons. Excitation of the valence shell electrons observed at the moment of x-ray radiation induced by ions of the energy level ≥ 5 MeV/u expressly indicates charge potential neutralization of the track core on the femtosecond time scale, following direct ion-atom interaction. This means that nano-plasma structures which could trigger severe deformations of the stopping medium material are not formed in early and mid phase of the ion stopping process [A4]. This conclusion seems to be groundbreaking for theoretical modelling of material deformations arising in consecutive phases of heavy ions stopping in solids.

4.3.4. Analysis of high-resolution x-ray spectra arising in plasma structures

Within a European research programme (Euratom) conducted on the largest tokamak in Europe (JET) intended for the research into selected plasma scenarios for ITER, I participated in the implementation of the project on high-resolution x-ray diagnostics modernization for the tokamak JET (Culham, Great Britain). The main aim of this modernization was providing the monitoring of x-ray radiation emitted by Ni^{26+}, Mo^{32+}, and W^{45+} as well as W^{46+} ions from the central plasma of the JET tokamak. The construction of a spectrometer, which was designed within the project, was to enable two extract two spectral groups of emission diagrams for three consecutive reflection orders (6 energy ranges, 3 per each spectral group). Each of two spectra groups is recorded in an individually intended diagnostic line. Diagnostic lines are separated from each other with a transverse vertical plane, which enables independent recording of a selected spectral group. According to the best knowledge of the author of this summary, this has been the first such a construction in the world ever.

The JET High-Resolution X-ray Spectrometer

W: Beryllium window on Octant 8

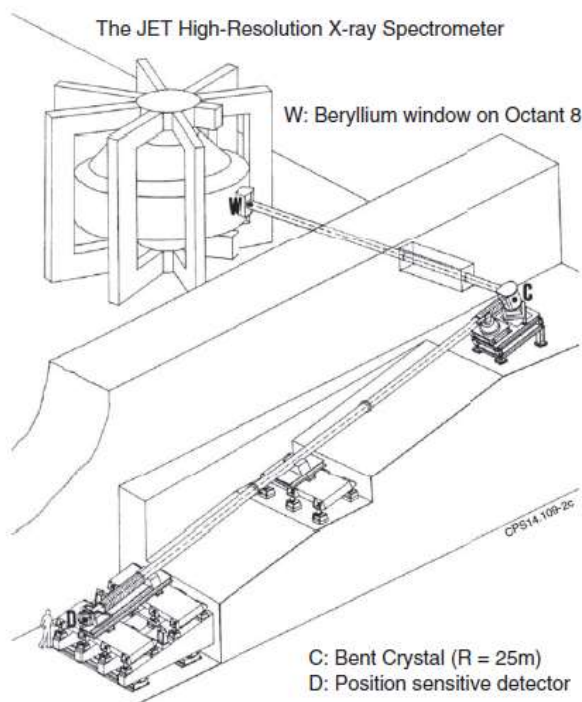C: Bent Crystal (R = 25m)
D: Position sensitive detector

Figure 12. The construction diagram of high-resolution x-ray spectrometer installed on the JET tokamak [A7].

The construction of the spectrometer is based on the so-called the circle Johann geometry with a Rowland circle of diameter R=12.5 m and two 20 m long metal pipes for 'transporting' x-ray photons from the JET tokamak to the chamber with diffraction crystals, and then to gas x-ray detectors. The construction diagram of the high-resolution x-ray spectrometer installed on the JET tokamak is shown in Figure 12. Metal pipes separated with a transverse vertical plane to obtain two independent diagnostic channels (upper and lower).

Upper diagnostic channel, equipped with SiO_2 crystal ($10\underline{1}1$) of a constant crystal lattice 2d=0.668 nm, was designed to monitor radiation emitted by Mo^{32+} and $W^{45+,46+}$ ions in 5.0-5.3 Å spectral range (in the first diffraction order). Lower diagnostic channel equipped with Ge crystal (220) (2d = 0.400 nm) was adapted to measurements in 1.5-1.6 Å spectral range (in the second diffraction order). The crystals sizes are 230x35x5 mm. They are cylindrically bent with 24.98 m bend radius.
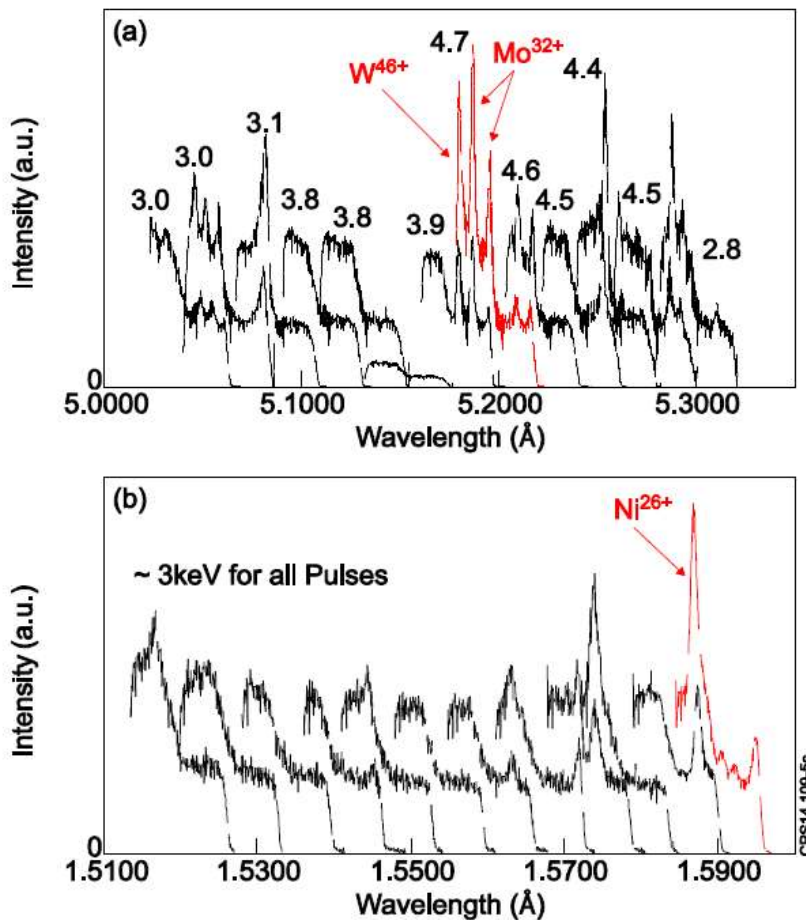

Figure 13. Spectral range of high-resolution x-ray diagnostics for (a) upper diagnostic canal (measurements of Mo^{32+} and $W^{45+,46+}$ lines) and (b) lower diagnostic canal (measurements of $Ni^{25+,26+}$ lines) [A7].

At the ends of diagnostic channels there are installed two gas detectors of GEM type, i.e. sensitive to both energy and position of the recorded photons. Detectors' energy resolution enables recording spectral diagrams in chosen diffraction orders. Appropriate position sensitivity, on the other hand, allows to record spectra in exceptionally high spectral (energy) resolution comparable with natural widths of recorded x-ray lines ($\lambda/\Delta\lambda \geq 1,2 \times 10^3$). GEM detectors were so designed, built and calibrated that they met the following requirements: covering of relatively large detection area (206x92 mm^2), position sensitivity not worse than 0.7 mm, high charge enhancement, detection stability for a wide range of photon flux, proper

energy resolution (not worse than 30% while maintaining position sensitivity) and time resolution not worse than 10 ms. To optimize detection capacity, Ar with CO_2 additive (15-30%) was chosen from the investigated selection of working mixtures of gases. Owing to the use of thin mylar foil as a material for the window of the detector, there was obtained 20-45% of performance capacity more as recording of x-ray radiation in soft x-ray radiation range (2-8 keV) is concerned [A6].

Figure 13 shows the full spectral range of high-resolution x-ray diagnostics recorded by GEM type detectors in both diagnostic channels, respectively, in the first and second diffraction order. For both diagnostic channels sensitivities were determined which control for: photon transmission in respective diagnostic channels, performance capacity of the detectors and diffraction indices of the crystals. The obtained response functions were additionally verified with the analyses of the intensity of constant radiation emitted from the JET tokamak and registered in the first three diffraction orders [A7]. This enabled precise analyses of absolute values of metallic impurities in the central plasma of the JET tokamak.
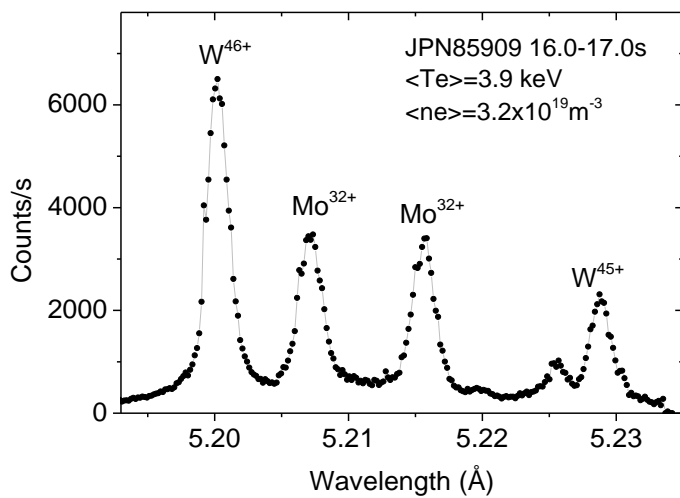

Figure 14. An x-ray spectrum of tungsten ($W^{45+,46+}$) and molybdenum (Mo^{32+}) ions registered on the JET tokamak in between 16 and 17 s of plasma discharge No. 85909 [A12].

X-ray spectra obtained with modified high-resolution x-ray diagnostics were the subject of advance analyses. In particular, tungsten ions spectra which are characterized by exceptionally complex structure [A8]. An attempt to reconstruct the spectra measured with the use of x-ray spectrometer installed on JET was necessary for proper interpretation of the measured tungsten spectra. An example of a spectrum measured upon one of plasma discharges on the JET tokamak (No. 85909) between 16-17 s is presented in Figure 14. The spectrum was measured in steady-state plasma in the mean temperature of $<T_e> \sim 3.9$ keV and $<n_e> \sim 3.2 \times 10^{19}$ m^{-3} electron density. Full temperature and electron density profiles as a function of the JET tokamak's radial radius is presented in Figure 15. It is clearly seen that both temperature and electron density profiles are nearly constant in the plasma discharge period under consideration. Only such plasma conditions allow advanced calibration analyses and form a benchmark for theoretical models.

Verification of measured x-ray structures and energy calibration was the greatest challenge as regards interpretation of the spectra recorded with the use of high-resolution x-ray diagnostics installed on the JET tokamak. Since spectra recorded on the JET tokamak actually are a sum or spectra for various temperatures and electron densities (from high T_e i n_e values in the central plasma to low values in the edge plasma), such a verification (calibration) is substantially limited in measurement uncertainty reduction. Furthermore, x-ray spectra recorded on the tokamak are affected by Doppler shifts, which increases measurement

uncertainty. For this reason, separate measurements, without Doppler shifts, had to be conducted under controlled temperature and electron density. Such conditions were possible to obtain with electron beam ion traps (EBIT).
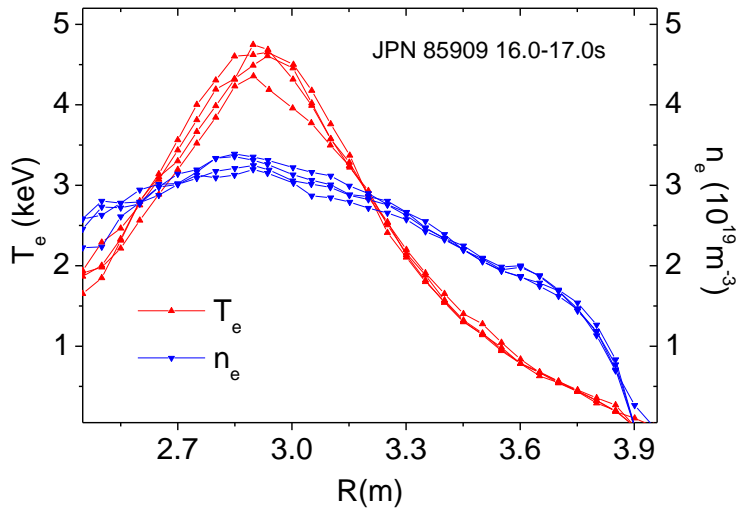

Figure 15. Temperature and electron density profiles as a function of the JET tokamak's radial radius [A12].
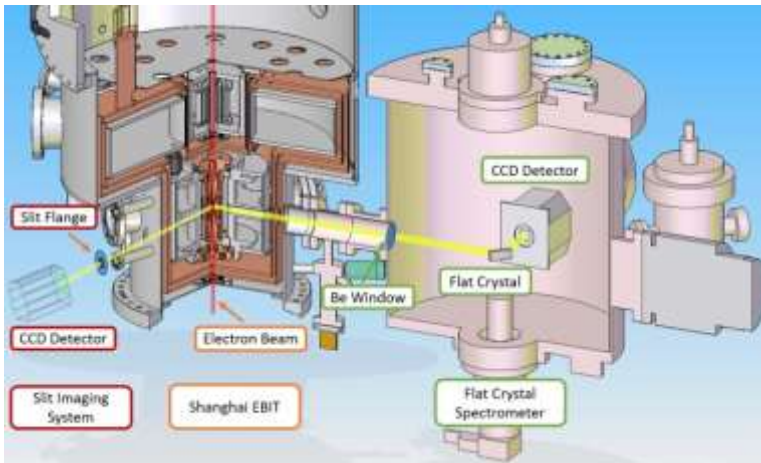

Figure 16. A general scheme of the experimental setup at the upgraded Shanghai EBIT [A12].

Respective tungsten W^{45+} and W^{46+} ions x-ray spectra measurements were carried out using EBIT in Shanghai (China). The general scheme of the experimental setup at the upgraded Shanghai EBIT is shown in Figure 16. Highly ionized tungsten ions were induced by monoenergetic electron beam of energy level range from 3.16 keV to 4.55 keV (the electron-beam energy distribution at its half maximum was below 50 eV), at a current 15–70 mA, which corresponds to 2.5–11.6 x 10^{18}m^{-3} electron density. X-ray spectra emitted by tungsten ions were recorded with a crystal spectrometer. The spectrometer had an installed Si <111> crystal, size of 5.0×2.5×0.5 cm^3, a crystal lattice 2d = 6.2712 Å and a CCD camera of 2048 × 2048 pixels (size of a single pixel x = 13.5μm). The spectral resolution of the spectrometer was not worse than $\lambda/\Delta\lambda \approx 4200$ in the wavelength range under consideration.

Figure 17 shows x-ray spectra of tungsten ions (Ni- and Cu-like) induced by electron beam of the energy level from 3.16 to 4.55 keV recorded with a crystal spectrometer installed at the EBIT. It can be seen in the Figure that x-ray spectra corresponding to $4d_{5/2} \rightarrow 3p_{3/2}$ electron transition in nickel-like tungsten ions (Ni1) dominate over copper- and nickel-like lines (Cu1, Cu2, Cu3 and Ni2) in all measured spectra. Such spectral structure remains in agreement with theoretical predictions.
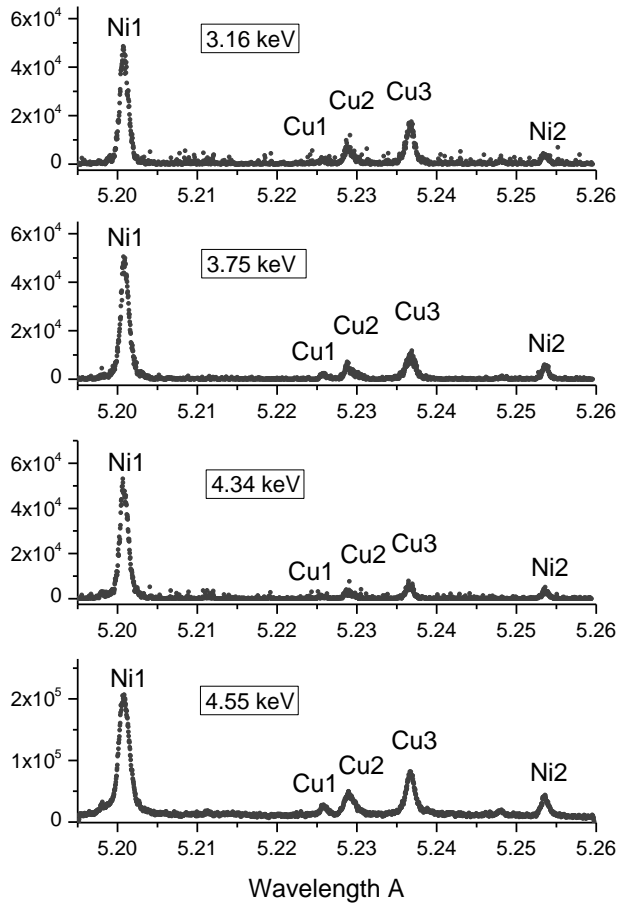
Figure 17. X-ray spectra of (nickel- and copper-like) tungsten ions induced by an electron beam of energy level from 3.16 to 4.55 keV recorded with crystal spectrometer installed at the EBIT type system in Shanghai [A12].

Energy (spectral) calibration was possible after initial identification of the x-ray lines. A linear relationship between the detector channel number (pixel) and the length of spectral waves was adopted due to the very narrow (5.19–5.26 Å) spectral range of the spectrometer. In the first step, the reference wavelengths of the National Institute of Standards and Technology (NIST) were bound to the peak centroids obtained with the use of the Gaussian fit for all transitions recorded in the copper- and nickel-like tungsten. By the comparison of NIST reference values for Ni1 and Ni2 lines defining the range of recorded radiation with their corresponding wavelengths obtained from the linear fit, it was possible to determine precision of the relative spectral scale for 0.3 Å per pixel (interval value between pixels $\Delta x = \Delta\lambda$).

Having determined relative calibration of the spectrometer, absolute calibration required a measurement of a single x-ray line in the recorded spectral range. In order to do that Ly-$\beta_{1,2}$ ($3p_{3/2}$-1s i $3p_{1/2}$-1s) lines of hydrogen-like silica (Si) ions were measured. Wavelengths of hydrogen-like lines are used as the most precise atomic reference because their x-ray spectra are exceptionally 'pure' (x-ray structure free of other spectra constituents that are related to the so-called satellite transitions). Calibration measurement was carried out with the electron beam of 4,6 keV energy and at a 70 mA current. Through bounding theoretical Ly-$\beta_{1,2}$ lines, calculated with the Multiconfiguration Dirac–Fock and General Matrix Elements (MCDFGME) code, to the pixels which correspond to Gaussian peaks centroids, the experimental uncertainty value was determined, as equal to 0.023 mÅ [A12].

So precise calibration allowed amazingly accurate determination (0.3–0.4 mÅ) of all considered wavelenghts of copper- and nickel-like (Ni2, Ni2, Cu1, Cu2 and Cu3) lines [A12]. It is worth to emphasize that in comparison with past NIST experimental values, with this method experimental uncertainty values were reduced by the factor of at least 3 (from the value 0.9–1.7 mÅ to 0.3–0.4 mÅ). According to my best knowledge, so far, it is the most precise measurement of these lines for tungsten ions within the wavelength range under consideration. In addition, Cu1 line wavelength corresponding to $[3p^5 3d^{10} 4s4d \, (3/2,2)_{3/2} \rightarrow 3d^{10}4s \, {}^2S_{1/2}]$ x-ray transition has been measured for the first time. Results for all the lines under consideration have been cited in the NIST database.

Verification and energy calibration of x-ray spectra recorded in the EBIT enabled a detailed analysis of spectra recorded on the JET tokamak. In the referential analysis for the spectra induced by plasma excitation No.85909 on the JET tokamak, upon determining proper wavelengths of individual x-ray lines of tungsten ions there was established a $\Delta\lambda \sim 0.7$-0.8 mÅ correction for the Doppler shift. The correction was determined on the basis of the JET central plasma rotation velocity not exceeding the value of 10 krad/s. Calibration procedure for the spectra recorded on the JET tokamak was based on neon-like molybdenum E1 and M2 x-ray lines which can be determined with MCDF-RCI (5.2076 and 5.2162 Å) calculations. In the calibration procedure, the same toroidal rotation velocity was used for tungsten and molybdenum ions in the central plasma of the JET tokamak.

Uncertainty of referential wavelengths were estimated from the comparison of MCDF-RCI calculations with the those obtained by means of relativistic multi-body perturbation mode and with the experimental values recommended by NIST. Eventually, the maximum difference between experimental and theoretical values, equal $\Delta\lambda_{ref} \sim 0.7$ mÅ, was used as the uncertainty of the wavelengths of molybdenum E1 and M2 lines. On the basis of the molybdenum E1 and M2 lines referential values and their uncertainties, nickel- and copper-like tungsten ions wavelengths were determined with the $\Delta\lambda = 0.9$ mÅ accuracy [A12]. It is worth emphasizing here that to my best knowledge these spectral values for $W^{45+, 46+}$ ions under tokamak plasma conditions have been by far the most precise ever obtained.

Experimental values determination was accompanied by advanced theoretical studies whose aim was to reconstruct x-ray spectra recorded on the JET tokamak and in the EBIT. Preliminary theoretical reconstruction of the x-ray spectra measured on the JET tokamak was performed by the FAC code. The code uses relativistic Dirac–Fock–Slater model to calculate respective atomic structures [B21]. According to theoretical simulations, all contributive factors that stem from individual electron configurations for all existing tungsten ions charge states, including open-shell W^{45+} and W^{47+} configurations in particular, have to be included in order to reconstruct x-ray spectra arising in plasma structures generated in JET tokamak operated with ~4 keV temperatures and $\sim 3 \times 10^{19} \, m^{-3}$ electron densities [A8].

In the next step of theoretical reconstruction of the spectra arising on the JET tokamak and in the EBIT type system there were performed advance calculations of the energy and intensity of respective x-ray transitions. MCDF code, which controls for Breit interaction and QED corrections as well as the FAC package were used for the calculations. In order to increase the accuracy of wavelengths calculations, the base of configuration state functions (CSFs) was enlarged, including the so-called virtual excited states in MCDF-RCI counts. CSFs base was systematically enlarged from the base (without the inclusion of virtual excited states) to an enlarged base that included virtual excited states of the main quantum number n=4-7 and the orbital quantum number l=0-4. Singular and double virtual excited states from 3s, 3p, 3d and 4d orbitals were taken into consideration for the nickel-like tungsten ions. Taking into account respective virtual excited states of copper-like tungsten ions is greatly hindered due to open-shell structure of these ions. Therefore, in this case, singular and double virtual excited states was divided into two groups: valence electron excitation (Valence-

Valence) and core electron excitation (Core-Valence). In this manner, the coincidence for consecutive enlarged CSFs bases, up to n=7 was obtained. Obtaining such a coincidence value points to the use of proper methodology of MCDF-RCI calculations. So performed MCDF-RCI calculations allowed to reconstruct the wavelengths of nickel- and copper-like tungsten ions spectral lines with previously unattainable accuracy. The progress of experimental accuracy and theoretical predictions of the present studies is shown in Figure 18. Significant underestimation of experimental wavelengths by previous theoretical MCDF and FAC predictions which do not control for CSFs correlations is clearly seen in the figure.
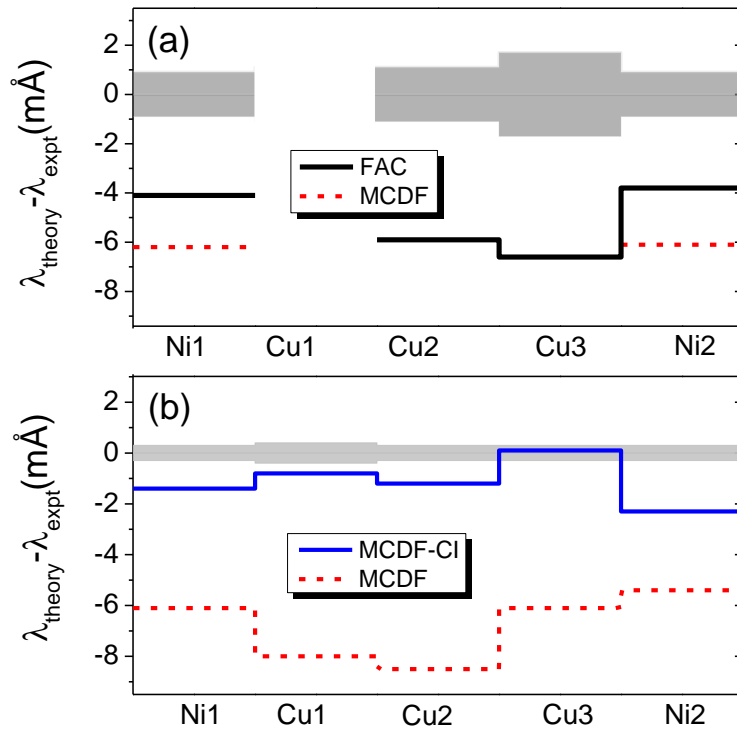

Figure 18. The comparison of (a) previous and (b) current theoretical and experimental wavelengths of nickel- and copper-like tungsten ions for 5.20-5.26 Å spectral range. Experimental uncertainties are marked as the grey hatched area [A12].

Figure 18(b) highlights not only the markedly improved accuracy of the measured wavelengths, from 0.9-1.7 mÅ to 0.3-0.4 mÅ, but also shows significantly greater agreement between new theoretical predictions and new experimental results obtained with the EBIT system. The most precise MCDF-CI calculations which take into account singular and double electron excitations to virtual states with the main quantum number up to do n=7 decrease discrepancies between the theory and experiment to the value below 1.5-2.5 mÅ [A12].

4.3.5. Determination of optimal conditions for the observation of the isomer state excitation by electron capture into an unfilled electron shell of an atom.

As it was mentioned in part 4.2, nuclear isomers, i.e. meta-stable excited nuclear states have unique ability to store great amounts of energy for a very long time. Thus, they are very attractive potential effective energy sources of new generation. Their capacity can be several orders of magnitude higher than of the most effective current chemical sources. In order for

these isomers to be applied as nuclear batteries, however, there is not only a need for us to learn how to 'charge' them, but also how to release the energy stored in them on demand.

One of the possible mechanisms of energy release from the isomeric state is by exciting it to the intermediate state (which is able to de-excite to the basic state almost instantly) as a result of the NEEC process. The NEEC process was the subject of detailed theoretical studies, which, inter alia, aimed at observing it experimentally for the first time. All previous attempts to observe the NEEC process experimentally, including the experiment with the use of the EBIT and [242]Am ions [B22], the experiment with a beam of [57]Fe ions penetrating Si crystal [B23], or, finally, plasma experiments, failed.
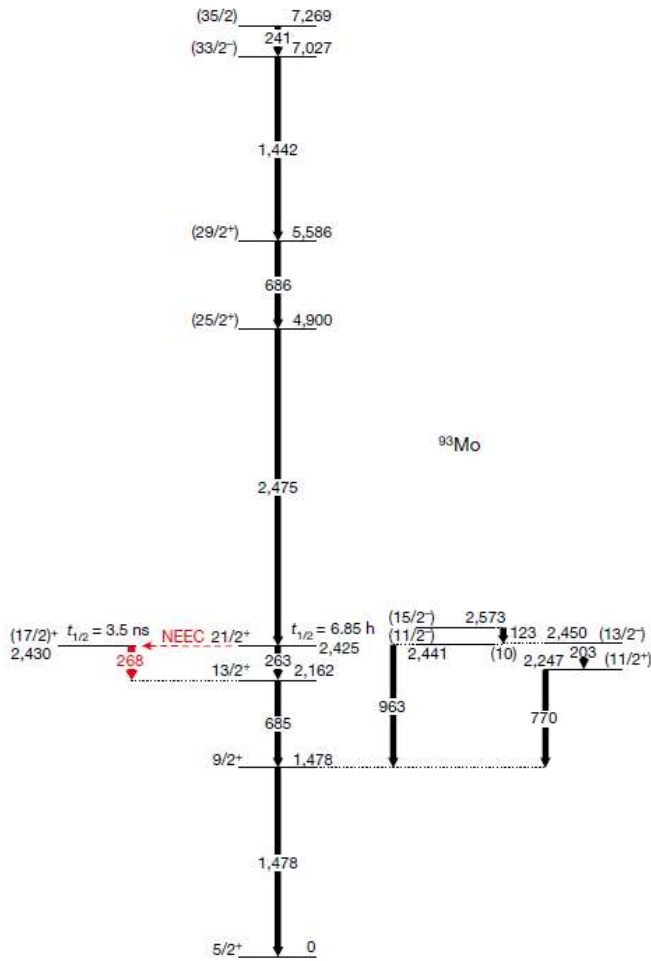

Figure 19. The simplified diagram of nuclear levels in [93]Mo [A11].

Therefore, I and my co-researchers undertook the challenge of designing an experiment to prove the existence of NEEC. In order to do that we adjusted and developed the idea of the experiment which was originally proposed by Karamian and Carrol in 2012 and based on the use of heavy ions and a target [B24]. Theoretical considerations were focused on the [93]Mo nuclei which can exist in the isomeric state [93m]Mo $21/2^+$ (spin 21 and parity + 1), 2.425 MeV energy, half-life life $T_{1/2}$=6.85 h. The isomeric state can be excited to the so-called intermediate state located only 4.85 keV above the isomeric state. The simplified diagram of nuclear levels in [93]Mo nuclei is represented by Figure 19. Sequential decay of the intermediate state to the basic state ($T_{1/2} \approx 3.5$ ns) allows the release of the energy which was originally accumulated in the isomeric state. Furthermore, the observation of $17/2^+ \rightarrow 13/2^+$ transition, of 267.9 keV, enables unequivocal identification of the NEEC process as this

transition is not possible without the change of the decay chain as a result of the NEEC process.

Following nuclear decay analysis, whose recording enables unequivocal the NEEC recording, it was necessary to make a preliminary experimental scenario. The aim of this scenario was the creation of ^{93m}Mo isomer in the first target and then, the observation of the NEEC in the second target (stopping medium) where ions were to be properly stopped so that it could obtain the kinetic resonance energy. In order to select a proper primary ions beam as well as the target, multiple cross sections calculations were carried out for fusion-evaporation nuclear reactions. The examples of calculations of cross sections for the $^{92-94}$Mo isotopes production (including ^{93m}Mo isomeric state production) done with the use of PACE4 [B25] code are shown in Figure 20. In case of ^{91}Zr+^{4}He reaction ^{93}Mo isotope production exceeds other isotopes' production within the vast range of the beam energy, where the isomeric ^{93m}Mo state production is the most effective within 6.6-7.7 MeV/A beam energy range [A10]. Similar calculations were performed for a few other reactions, out of which ^{90}Zr+^{7}Li reaction was chosen for the experiments.
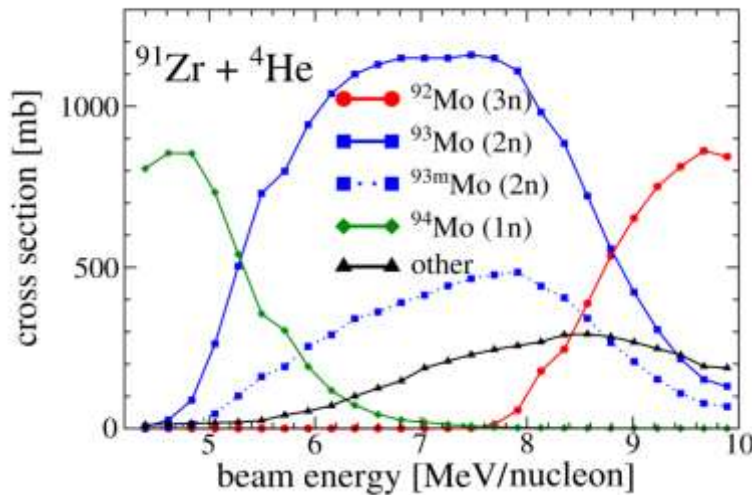

Figure 20. Cross-sections for $^{92-94}$Mo isotopes production (including isomeric^{93m}Mo state) as a function of the beam energy for ^{91}Zr+^{4}He reaction, calculated with PACE4 [A10].

In the next step of the analyses, mean charge states of ^{93m}Mo ions as a function of their kinetic energy for light targets: gas (^{4}He) and solid (^{12}C) and energies of the orbitals corresponding to kinetic resonance energies necessary for the NEEC. Figure 21 clearly shows that the predicted mean charge states (green, constant line) monotonically decrease during ^{93m}Mo stopping in the helium as in carbon target. It is also noticeable that a little higher mean charge states occur in ^{12}C target than ^{4}He, for a given kinetic energy of ^{93m}Mo ions. Higher charge states are conducive for the NEEC effectiveness as they provide higher number of unfilled orbitals into which the target's electrons can be captured. The energies released by electron capture for selected charge states were determined on the basis of MCDF calculations of binding energies of M and N orbitals. In the next step, all possible NEEC resonance energies, i.e. ions' kinetic energies of within the range of charge states from q=+32 up to q=+36, where electron capture into a given sub-shell may cause isomeric excitation, were estimated.

Having determined proper combination of charge states of ^{93m}Mo stopping ions in low-Z targets and their kinetic resonance energies at which electron capture releases the proper amount of energy ($\Delta E = 4{,}85$ keV) needed to excite an isomeric $21/2^{+}$ state to an intermediate $17/2^{+}$ one, we went on to plan the experiment with the use of a heavy ions linear accelerator ATLAS in Argonne National Laboratory (USA). ^{90}Zr ions of initial energy 840

MeV and a system of targets were used in the experiment (Figure 22). The targets were particularly designed to produce ^{93m}Mo ions (^{7}Li target) and to the process of NEEC itself (^{12}C target). A 3-mm gap between ^{7}Li and ^{12}C targets enabled additional production of isomeric states via fast (picosecond time regimes) decays of high-spin states to the $21/2^+$ isomeric state. 2475 keV, $25/2^+ \rightarrow 21/2^+$ transition is one of such transitions (see Figure 19).
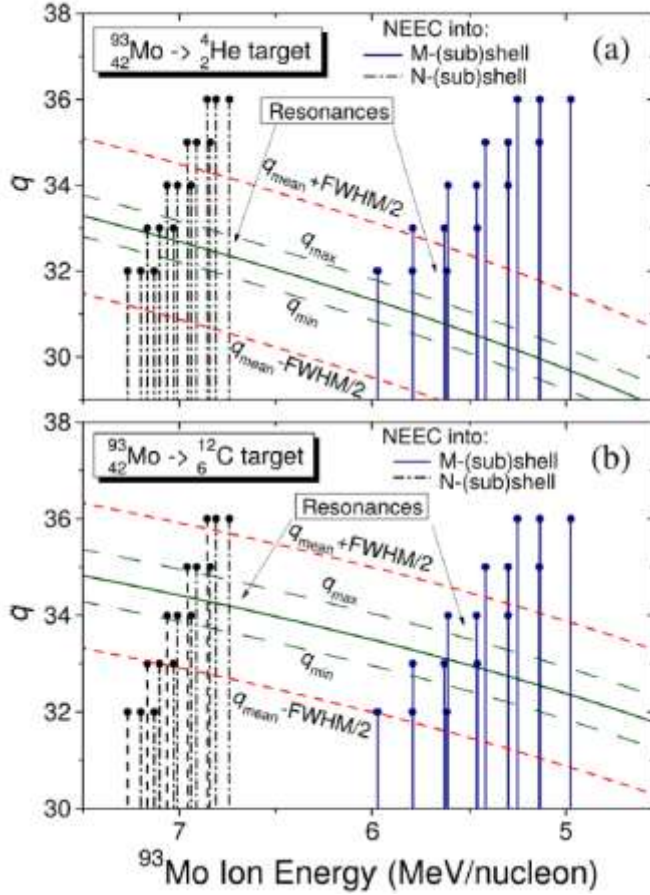

Figure 21. Mean charge states of ^{93m}Mo ions as a function of their kinetic energy for (a) ^{4}He target and (b) ^{12}C target [A10].

The targets' system was installed centrally in the *Gammasphere* spectrometric system composed of 96 germanium detectors (Ge high-purity) arranged in 16 rings. Such system enables performance of even three-fold coincidence analyses which in fact reduce systematic measurement errors related to coincidental recording of a given nuclear transition. Energetic conditions or thresholds were laid down on the specific nuclear transitions (the so-called gates) in the coincidence analyses. In order to identify NEEC, a coincidence condition was laid down on 2475 keV, $25/2^+ \rightarrow 21/2^+$ and 1478 keV, $9/2^+ \rightarrow 5/2^+$ transitions and $17/2^+ \rightarrow 13/2^+$ as well as $13/2^+ \rightarrow 9/2^+$ were observed, of energies 268 keV and 685 keV, respectively. [Figure 23(a)]. 268 keV $17/2^+ \rightarrow 13/2^+$ transition was observed in coincidence with power supplying to $(25/2^+ \rightarrow 21/2^+)$ and $13/2^+ \rightarrow 9/2^+$ isomeric state, with statistic 7σ over the background. A similar coincidence analysis for 2475-keV and 268-keV transitions allowed to observe 685-keV $(13/2^+ \rightarrow 9/2^+)$ and 1478-keV $(9/2^+ \rightarrow 5/2^+)$, as it can be seen in Figure 23(c). In addition, for comparison, Figure 23(b) shows coincidence spectrum with one condition laid down on 1478-keV $(9/2^+ \rightarrow 5/2^+)$ transition.
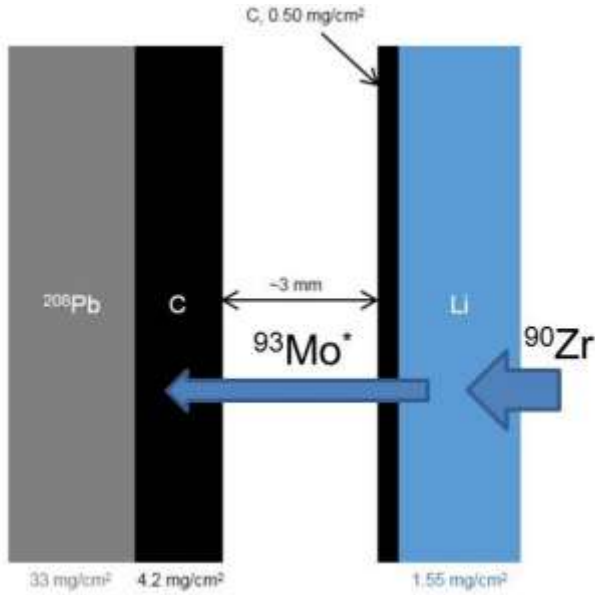
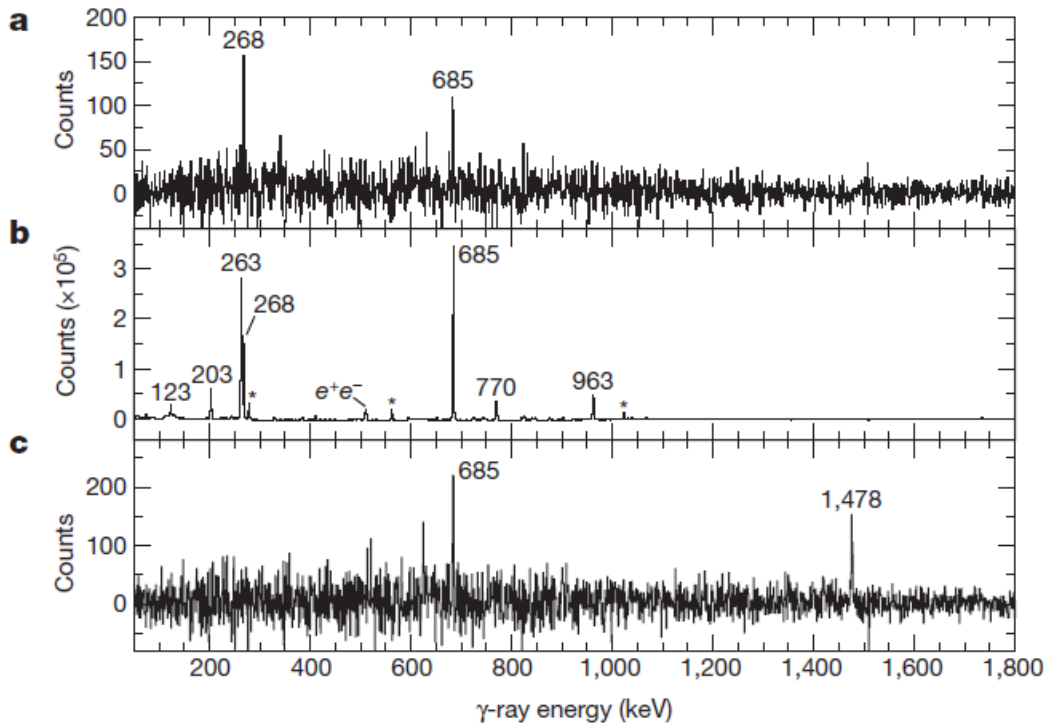Figure 22. System of the targets used in the NEEC experiment [A11].

Figure 23. Gamma radiation spectra showing the NEEC signature in ^{93m}Mo isomer; (a) the coincidence spectrum with a double condition on 2475-keV ($25/2^+ \rightarrow 21/2^+$) and 1478-keV ($9/2+ \rightarrow 5/2+$) transitions; (b) the coincidence spectrum with a singular condition on 1478-keV ($9/2+ \rightarrow 5/2+$) transition; (c) the coincidence spectrum with a double condition on 2475-keV ($25/2+ \rightarrow 21/2+$) and 268-keV ($17/2+ \rightarrow 13/2+$) transitions [A11].

Results of the present analyses clearly indicate coincidences between 2475-keV ($25/2^+ \rightarrow 21/2^+$) transition supplying the isomeric state and the sequence of 268-keV ($17/2^+ \rightarrow 13/2^+$) $\rightarrow$ 685-keV ($13/2^+ \rightarrow 9/2^+$) $\rightarrow$ 1478-keV ($9/2^+ \rightarrow 5/2^+$) gamma transitions leading to the decay of the intermediate state ($17/2^+$) to the basic state ($5/2^+$). The sequence of such transitions is impossible without isomeric state excitation to the intermediate state (isometric state life time $T_{1/2}$=6,85 h) and, thus, is an unequivocal signature of isometric state depopulation that is ascribed to NEEC.

In order to determine probability of the $(21/2^+)$ isomeric state excitation to $(17/2^+)$ intermediate state, the analysis of two coincidence spectra was conducted:

➢ a coincidence spectrum with double conditions laid down on 241-keV $(35/2 \rightarrow 33/2^-)$ and 1478-keV $(9/2^+ \rightarrow 5/2^+)$ transitions, the power supplying of the isomeric state and the NEEC process, and

➢ a coincidence spectrum with double conditions laid down on 241-keV $(35/2 \rightarrow 33/2^-)$ and 686-keV $(29/2^+ \rightarrow 25/2^+)$ transitions, which corresponds to the power supplying of only the isomeric state.

Due to the lack of any other decay chain of the γ 268-keV energy transition, apart from that which covers isomeric state excitation, the ratio between the areas under the peaks of gamma line, 268-keV and 2475-keV, (adjusted to the detection system capacity) should directly determine the probability of NEEC in the carbon target. So determined probability was $P_{exc}^{NEEC}(21/2^+) = 1\% \pm 0,3\%$ for the 4.2 mg/cm^2 thick carbon target. On the basis of the determined probability of NEEC P_{exc}^{NEEC} also averaged to the target's thickness respective cross-section was also determined $\sigma_{exc}^{NEEC}(21/2^+) \approx 40 \ b$ [A11]. Both values are the first in the world experimental values concerning the NEEC process that have been published. Here, it is worth to emphasize that theoretical predictions on cross-sections on NEEC are different from each other by many orders of magnitude. Therefore, the first experimental results pose a challenge for all theoretical models that are being developed.

The first observation of isomeric state depopulation ascribed to NEEC [A11] and so large discrepancies as regards theoretical predictions inclined me to undertake further studies in the field. As a results of this work, a new experimental scenario based on the ion-atom interaction for the isomeric state ($T_{1/2}$ = 141 yr, $I^\pi = 5^-$) existing in ^{242}Am nuclei has been prepared [A14]. In earlier theoretical studies of Pálffy et al. [B13], it was shown that the depopulation of the ^{242m}Am isomeric state as a result of the electron capture and associated excitation of the isomeric state (through a low energy transition E2, ΔE~4,1 keV) into the intermediate state $I^\pi = 3^-$ can be about two orders of magnitude more efficient than the ^{93m}Mo depopulation that was experimentally observed.
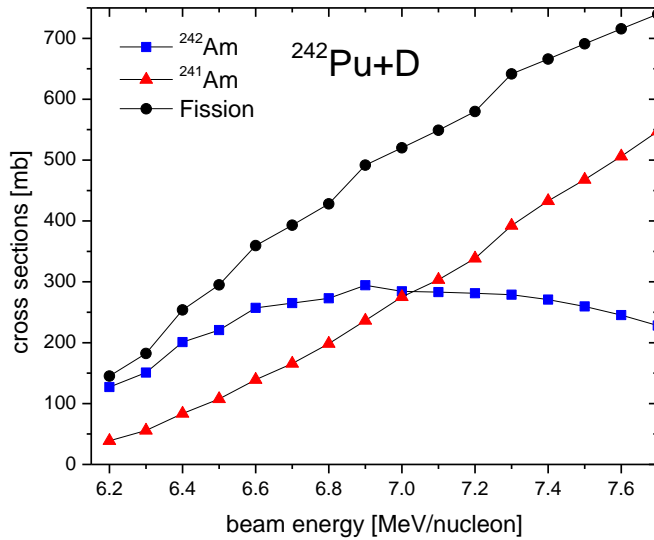

Figure 24. Cross section for the ^{242}Pu + ^{2}D beam-target reaction as a function of the beam energy, calculated with the GEMINI++ code [A14].

In the recently published article [A14], I identified with my co-reserchers optimal experimental conditions both for the creation of the ^{242m}Am isomeric state as well as for the NEEC process in light solid targets. In order to ensure the effective production of ^{242}Am nuclei, including ^{242m}Am isomeric states, the cross-sections were calculated for ^{242}Pu + ^{2}D and ^{238}U + ^{7}Li nuclear reactions (fusion-evaporation reactions) by means of the GEMINI++ code

[B26]. The results of these calculations clearly showed that the ^{242}Pu + ^{2}D reaction allows for the effective production of ^{242}Am nuclei at ~ 7 MeV/A ion beam energy with the cross-section of almost 300 mb (Figure 24).
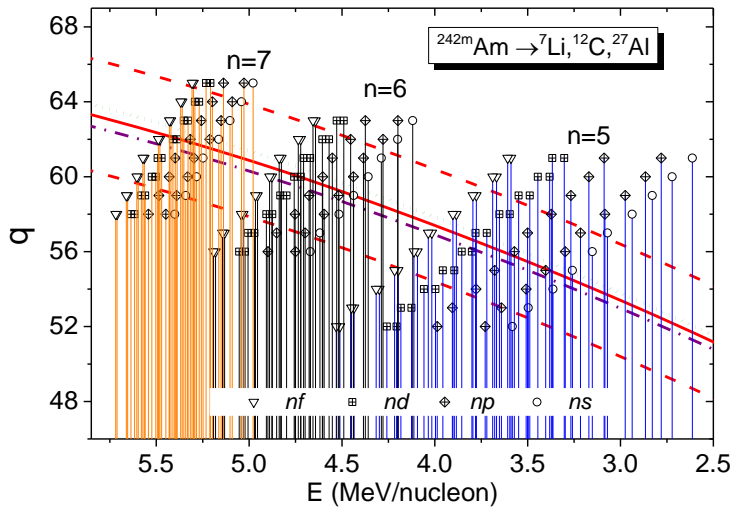

Figure 25. The qmean of the ^{242m}Am projectile as a function of its kinetic energy for ^{7}Li (green dotted line), ^{12}C (red solid line), and ^{27}Al (purple dash-dotted line) stopping media [A14].

As part of work on the optimal atomic conditions necessary for the NEEC process to take place, the average charge states of ^{242m}Am ions were determined as a function of their kinetic energy for selected solid targets (^{7}Li, ^{12}C, and ^{27}Al). In the next step, based on calculated binding energies for subshells n = 5, n = 6 and n = 7 using the FAC code [B21] the resonant kinetic energies of ^{242m}Am ions have been determined for which the NEEC process becomes possible (Figure 25). The figure also shows two red dashed lines that define the area of charge state distribution for ^{242m}Am ions penetrating the ^{12}C target ($\Delta q \sim \pm 3$). The area defines the group of expected charge states for which the NEEC process for a given kinetic resonant energy is most likely to occur.

It should be emphasized that in this work I proposed a new original approach to determine the theoretical predictions of resonance strengths for excitations of the ^{242m}Am isomeric state as a result of the NEEC process for capture into particular subshells (subshells with n=5, 6 i 7), for initial dominant electronic configurations and ion charge states of ^{242m}Am. Using the developed method, it was possible to determine the theoretical resonant strengths for the capture into individual subshells as a function of ^{242m}Am ion energy This work has determined optimal experimental conditions as well for ^{242m}Am isomeric state production as for NEEC in light solid targets. Moreover, within the framework of this work it was possible to set theoretical predictions of the so-called resonance strengths for dominant electron configurations and charge states as a function of ^{242m}Am ions energy. The result of these studies is illustrated by Figure 26. It was shown that the highest partial contributions to the NEEC process in the beam-based scenario should come from captures into 5p and 6p subshells of ^{242m}Am ions with charge states from q ≈ +54 to q ≈ +62 at kinetic energies of 3.0–5.0 MeV/nucleon. High partial contributions to NEEC from captures into 7p subshells at the kinetic energies above ≈5 MeV/nucleon are also available due to the high beam energy requirement needed to obtain the largest possible cross sections for the ^{242}Am isotope production, especially for the ^{242}Pu + ^{2}D beam-target reaction. Electron captures into *ns* and *nd* subshells should give much smaller contributions to the NEEC process than those into *np* ones, while captures into *nf* subshells seem to be negligible.
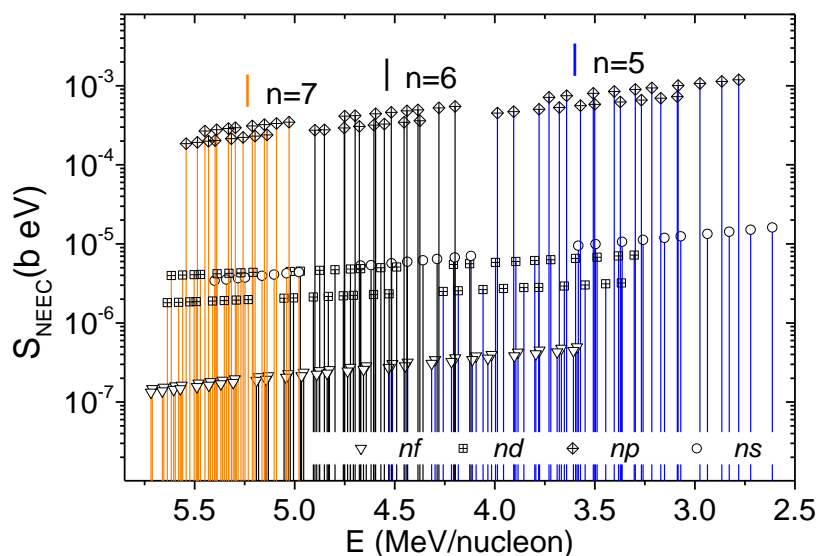
31

Figure 26. Resonance forces of isomeric state excitement due to the NEEC process $S_{NEEC}^{q,nlj}$ determined for dominant electron configurations (nl$_j$ n=5, 6 i 7) and charge states (q) as a function of ^{242m}Am ions energy [A14].

The results of this part of the study have been published in 3 articles ([A10], [A11] and [A14]) in the prestigious journals Nature and Physical Review C.

4.4. References (list B)

The set of sources cited in the summary.

[B1] A. Itoh, D. Schneider, T. Schneider, T. J. M. Zouros, G. Nolte, G. Schiwietz, W. Zeitz, and N. Stolterfoht, Phys. Rev. A 31 (1985) 684.

[B2] F.F. Komarov, Phys. Usp. 46 (2003) 1253.

[B3] P. Sigmund, Stopping of Heavy Ions, Springer Tracts of Modern Physics No. 204 (Springer, Berlin, 2004).

[B4] R. Kelly and M. Fernanda (eds.), Materials Modification by High-Fluence Ion Beams (Kluwer Academic, New York, 1989).

[B5] J. J. MacFarlane, P. Wang, J. Bailey, T. A. Mehlhorn, R. J.Dukart, and R. C. Mancini, Phys. Rev. E 47 (1993) 2748.

[B6] G. Kraft, Prog. Part. Nucl. Phys. 45 (2000) S473.

[B7] S. R. Elliott, P. Beiersdorfer, B. J. MacGowan, and J. Nilsen,Phys. Rev. A 52, 2689 (1995).

[B8] K. W. Hill, M. L. Bitter, S. D. Scott, A. Ince-Cushman, M.Reinke, J. E. Rice, P. Beiersdorfer, M. F. Gu, S. G. Lee, C.Broennimann, and E. F. Eikenberry, Rev. Sci. Instrum. 79,10E320 (2008).

[B9] P.M. Walker and G.D. Dracoulis, Nature 399, 35 (1999); P.M. Walker and J.J. Carroll, Physics Today 58-6, 39 (2005).

[B10] V. Goldanskii and V.A. Namiot, Phys. Lett. B 62 393 (1976).

[B11] J.H. Hamilton, Internal Conversion Processes (Ed. by J.H. Hamilton, Academic Press Inc., New York, 1966), p. 1ff, and references therein.

[B12] N. Cue, J.-C. Poizat, and J. Remillieux, Europhys. Lett. 8 19 (1989).

[B13] A. Pálffy, J. Evers, and C.H. Keitel, Phys. Rev. Lett. 99 172502 (2007).

[B14] S.A. Karamian and J.J. Carroll, Phys. Atomic Nucl. 75 1362 (2012).

[B15] R. Diamant et al., Phys. Rev. A 79, 062511 (2009).

[B16] W. Heisenberg, Z. Phys. 32 (1925) 841.

[B17] S. Goudsmit and L. Gropper, Phys. Rev. 38 (1931) 225.

[B18] W. Wölfli, C. Stoller, G. Bonani,M. Suter, and M. Stöckli, Phys.Rev. Lett. 35 (1975) 656.

[B19] J. Hoszowska, J.-Cl. Dousse, J. Szlachetko, Y. Kayser, W. Cao, P. Jagodziński, M. Kavcic, and S. H. Nowak, Phys. Rev. Lett.107 (2011) 053001.

[B20] A. V. Lankin, I. V. Morozov, G. E. Norman, S. A. Pikuz Jr., and I. Yu. Skobelev, Phys. Rev. E 79, 036407 (2009).

[B21] M. F. Gu, Can. J. Phys. 86, 675 (2008).

[B22] L. Bernstein, EBIT plans in Livermore and Berkeley, in Proceedings of the ECT Workshop on Atomic Effects in Nuclear Excitation and Decay, Trento, Italy, June 15–19, 2009 [www.ect.it, under link to meetings for 2009].

[B23] P. Morel, J. M. Daugas, G. Gosselin, V. Meot, and D. Gogny, AIP Conf. Proc. 769 (2005) 1085.

[B24] S. A. Karamian and J. J. Carroll, Phys. At. Nucl. 75 (2012) 1362.

[B25] O. B. Tarasov and D. Bazin, Nucl. Instrum. Meth. Phys. Res. B 204, 174 (2003).

[B26] R. J. Charity, Phys. Rev. C 82, 014610 (2010).

5. Other scientific accomplishments

5.1. Studies with the use of beams of uranium ions in the storage ring at GSI Darmstadt's laboratory

In the years of 2004 and 2005 in the framework of postdoc fellowship I participated in Prof. Thomas Stöhlker's atomic physics group in preparation to the experiments and in the various experiments carried out in the storage ring in the GSI laboratory in Darmstadt. Besides publications which constitute the basis of the habilitation procedure, this participation resulted also in other works on, among many others, x-ray Balmer series measurements of hydrogen-like uranium induced in the process of radiative recombination [C1], the studies on the characteristics of doubly excited $1s(2s)^2$ atomic decay in Li-like uranium ion (U^{89+}) [C2], the studies on the life times of low-charged uranium ions in the storage ring [C3] and on the measurements of hard x-ray radiation emitted by highly ionized uranium ions [C4].

5.2. Studies of the interaction between relativistic ^{3}He ions and carbon and gold targets

In the years 2005 and 2006 I participated in the studies of the cross-sections active for ionization and electron capture in relativistic ^{3}He ions with carbon (C) and gold (Au) targets. The experiment was carried on the cyclotron of the Research Center for Nuclear Physics in Osaka (Japan). The analysis of the obtained results allowed to determine the relations of single-ionized helium ions (^{3}He$^+$) to the intensities of doubly-ionized helium ions (^{3}He^{++}) as a function of the target's thickness. Extrapolation of the results for the zero thickness of C and Au targets allowed for determining the values of ionization cross-sections (stripping) and the electron capture. In case of ^{3}He^{++} interaction with the C target, owing to the use of the intensity measurement of ^{3}He$^+$ ions beam in coincidence with the photons coming from a radiative capture (of 84 keV energy) radiative and nonradiative contributive factors to the absolute cross-section for the electron capture were determined. The obtained results have

greatly expanded current systematics of atomic processes in high energies. It has been also indicated that the results obtained for radiative capture by totally ionized $^3He^{++}$ confirm the potential unique possibility of discovering entirely ionized matter in the intergalactic space. The results of these studies have been published in the journals in the ISI Master Journal List [C5], [C6].

5.3. Studies of x- ray spectra in mid-Z atoms induced by collisions with ions and by x-ray radiation.

In the years 2006-2018 I took part in x-ray spectra studies of mid-Z atoms induced by the collision with nitrogen and oxygen ions. Relevant measurements of spectra were performed on Philips cyclotron in Paula Scherrer's Institute (PSI) in Villigen (Switzerland), at which it was installed a high-resolution crystal spectrometer of *von Hamos* type. The presented studies led, inter alia, to the proposal of innovative approach to the description of complex L-line x-ray transitions which occur under highly ionized M-shell conditions. This enabled testing atomic models which were related both to the electron structure of an atom (MCDF calculations) and to ionization dynamics (calculated with a semi-classical method). It is also worth emphasizing that in the measurements of $L\alpha_{1,2}$ Pd series, hyper-satellite lines corresponding to the de-excitation of doubly ionized state in the L shell (L^{-2}) were observed for the first time. The results of these studies have been published in the journals in the ISI Master Journal List [C7], [C8], [C9], [C10]. In 2018, these publications were supplemented with a work on K^{-2} states de-excitation in metallic atoms *3d* (Ca, V, Fe and Cu) formed in the collisions with C ions of 10 MeV/nucleon [C11] and a work that analyses the asymmetry observed in high-resolution spectra of 3d atoms induced by x-ray radiation [C12].

5.4. Studies of x- ray spectra induced in impulse plasma

In the years from 2010 to 2016 I participated in the studies on x-ray spectra induced in impulse plasma. Participation in these studies resulted in the works concerning high-resolution x-ray spectra analysis. The x-ray spectra were induced on the Plasma-Focus device (PF-1000) in The Institute of Plasma Physics and Laser Microfusion in Warsaw (IFPiLM) during high-current discharges, on the Gamble II device of Naval Research Laboratory (NRL) in Washington (USA), with the use of Plasma-Filled Rod-Pinch (PFRP) diode; on the Z- machine device in Sandia National Laboratories, Albuquerque (USA) [C13], [C14], [C15], [C16], [C17], [C18], [C19], [C20], [C21], [C22].

5.5. Participation in the experiment campaigns of JET laboratory carried out under the European Programme of Fusion Studies Euratom

From 2008 to 2014, within the framework of the participation in Euratom Programme on the position of a responsible officer of high-resolution x-ray diagnostics in JET laboratory and later after returning to work in National Centre for Nuclear Research on the position of an adiunctus I took part in experimental campaigns conducted in JET laboratory within European Programme of Fusion Studies Euratom. Besides publications that are the basis of habilitation procedure, participation in these campaigns resulted in other publications on: the monitoring of the radiation emitted Be hydgrogen-like ions with the use of Bragg rotor spectrometer [C23], the level of metallic (Fe, Ni, Cu, Mo and W) impurities of the central plasma created during radio frequency or Neutral Beam Injection pulses [C24], [C25].

5.6. Development of gamma diagnostics for experimental thermonuclear reactors, including ITER

In the years 2012-2018 within EuroFusion project and the project of European F4E agency established for the coordination of the works connected with the research for the purpose of experimental thermonuclear reactor ITER I implemented tasks connected with the preparation of gamma camera for alpha particles monitoring (via the measurement of 4.4 MeV gamma radiation induced by the $^9Be(\alpha,n\gamma)^{12}C$ reaction and the so-called escape electrons (by constant x-ray spectrum measurement). In particular, with Prof. Marek Moszyński I prepared the report which compares properties of various scintillation detectors that may be used in gamma camera creation for ITER reactor. The results of these studies have been published in the journals in the ISI Master Journal list [C26], [C27], [C28], [C29], [C30].

6. Bibliogrphy (list C)

[C1]   **The Balmer Spectrum of H-like Uranium Produced by Radiative Recombination at Low-Velocities**, R. Reuschl, A Gumberidze, Th. Stohlker, C. Kozhuharov, **J. Rzadkiewicz**, U. Spillmann, S. Tashenov, **Radiation Physics And Chemistry 75** (2006) 1740.

[C2]   **Investigation of the Decay Properties of the 1s(2s)^2 State in Li-Like Uranium**, S. Trotsenko, Th. Stöhlker, D. Banas, C.Z. Dong, S. Fritzsche, A. Gumberidze, S. Hagmann, S. Hess, P. Indelicato, C. Kozhuharov, M. Nofal, R. Reuschl, **J. Rzadkiewicz**, U. Spillmann, A. Surzhykov, M. Trassinelli, G. Weber, **Journal of Physics: Conf. Series 58** (2007) 141.

[C3]   **Beam lifetimes for low-charge-state heavy ions in the GSI storage rings**, R. D. DuBois, O. de Lucio, M. Thomason, G. Weber, T. Stöhlker, K. Beckert, P. Beller, F. Bosch, C. Brandau, A. Gumberidze, S. Hagmann, C. Kozhuharov, F. Nolden, R. Reuschl, **J. Rzadkiewicz**, P. Spiller, U. Spillmann, M. Steck, S. Trotsenko, **Nucl. Instrum. Methods B 26** (2007) 230.

[C4]   **Crystal optics for hard-X-ray spectroscopy of highly charged ions,** H.F. Beyer, D. Attia, D. Banas, E.-O. Le Bigot, F. Bosch, J.-Cl. Dousse, E. Förster, A. Gumberidze, S. Hagmann, S. Heß, J. Hoszowska, P. Indelicato, P. Jagodzinski, Chr. Kozhuharov, Th. Krings, D. Liesen, X. Ma, B. Manil, I. Mohos, M. Pajek, D. Protić, R. Reuschl, **J. Rzadkiewicz**, A. Simionovici, U. Spillmann, Z. Stachura, Th. Stöhlker, M. Trassinelli, S. Trotsenko, A. Warczak, O. Wehrhan, E. Ziegler, **Spectrochimica Acta Part B: Atomic Spectroscopy 64**, (2009) 736.

[C5]   **Charge exchange processes for semi-relativistic helium ions ($\beta = 0.51$) in solid gold**, A. Gójska, D. Chmielewska, **J. Rzadkiewicz**, Z. Sujkowski, T. Adachi, H. Fujita, Y. Fujita, K. Hara, Y. Haruyama, J. Kamiya, H. Ogawa, M. Saito, Y. Shimizu, Y. Shimbara, M. Tanaka, H.P. Yoshida, I. Katayama, **Nucl. Instrum. Methods B 235** (2005) 368.

[C6]   **Radiative and non-radiative electron capture from carbon atoms by relativistic helium ions**, A. Gojska, D. Chmielewska, P. Rymuza, **J. Rzadkiewicz**, Z. Sujkowski, T. Adachi, H. Fujita, Y. Fujita, Y. Shimbara, K. Hara, Y. Shimizu, H. P. Yoshida, Y. Haruyama, J. Kamiya, H. Ogawa, M. Saito. M. Tanaka, **European Physics Journal A 27** (2006) 181.

[C7]   **Multiple Ionization Effects In X-Ray Emission Induced By Heavy Ions**, M. Czarnota, M. Pajek, D. Banaś, J.-Cl. Dousse, Y.-P. Maillard, O. Mauron, P. A. Raboud, M. Berset, D. Chmielewska, **J. Rzadkiewicz**, Z. Sujkowski, J. Hoszowska, K. Słabkowska, M. Polasik, **Brazilian Journal of Physics 36** (2006) 546.

[C8]   **High-resolution X-ray study of the multiple ionization of Pd atoms by fast oxygen ions**, M. Czarnota, D. Banaś, M. Berset, D. Chmielewska, J.-Cl. Dousse, J. Hoszowska,

Y.-P. Maillard, O. Mauron, M. Pajek, M. Polasik, P. A. Raboud, **J. Rzadkiewicz**, K. Słabkowska Z. Sujkowski, **Eur. Phys. J. D 57**, 321 (2010).

[C9] **Observation of internal structure of the L-shell x-ray hypersatellites for palladium atoms multiply ionized by fast oxygen ions,** M. Czarnota, D. Banaś, M. Berset, D. Chmielewska, J.-Cl. Dousse, J. Hoszowska, Y.-P. Maillard, O. Mauron, M. Pajek, M. Polasik, P. A. Raboud, **J. Rzadkiewicz**, K. Słabkowska, Z. Sujkowski, **Phys. Rev. A 81**, 064702 (2010).

[C10] **Satellite and hypersatellite structures of Lα1,2 and Lβ1 x-ray transitions in mid-Z atoms multiply ionized by fast oxygen ions**, M. Czarnota, D. Banas, M. Berset, D. Chmielewska, J.-Cl. Dousse, J. Hoszowska, Y.-P. Maillard, O. Mauron, M. Pajek, M. Polasik, P. A. Raboud, **J. Rzadkiewicz**, K. Słabkowska, Z. Sujkowski, **Physical Review A 88**, 052505 (2013).

[C11] **Hypersatellite x-ray decay of 3d hollow-K-shell atoms produced by heavy-ion impact**, Y.-P. Maillard, J.-Cl. Dousse, J. Hoszowska, M. Berset, O. Mauron, P.-A. Raboud, M. Kavčič, **J. Rzadkiewicz**, D. Banaś, K. Tökési, **Physical Review A 98**, 012705 (2018).

[C12] **Kα 1,2 x-ray linewidths, asymmetry indices, and [KM] shake probabilities in elements Ca to Ge and comparison with theory for Ca, Ti, and Ge**, Y. Ito, T. Tochio, H. Ohashi, M. Yamashita, S. Fukushima, M. Polasik, K. Słabkowska, Ł. Syrocki, E. Szymańska, **J. Rzadkiewicz**, P. Indelicato, J.P. Marques, M.C. Martins, J.P. Santos, F. Parente, **Phys. Rev. A 94** (2016) 042506.

[C13] **Spatially resolved high-resolution x-ray spectroscopy of high-current Plasma-Focus discharges,** S. Zając, **J. Rzadkiewicz**, O.Rosmej, M. Scholz, Zhao Yongtao, A. Gójska, M. Paduch, E. Zielińska, **Rev. Sci. Instrum. 81**, 10E312 (2010)

[C14] **Influence of multiple outer-shell electron stripping on the Kα and Kβ x-ray energies of iridium, J. Rzadkiewicz**, K. Słabkowska, M. Polasik, J. Starosta, E. Szymańska, K. Kozioł, M. Scholz, N. R. Pereira, **Phys. Scr. T156** (2013) 014083.

[C15] **Tungsten L transition line shapes and energy shifts resulting from ionization in warm dense matter**, John F. Seely, B.V. Weber, D.G. Phipps, N.R. Pereira, D. Mosher, K. Słabkowska, M. Polasik, J. Starosta, **J. Rzadkiewicz**, S. Hansen, Uri Feldman, L.T. Hudson, J.W. Schumer, **High Energy Density Physics 9** (2013) 354

[C16] **High-resolution (~0.05%) red shift of a ~ 60 keV Kb line upon ionization**, N.R. Pereira, B.V. Weber, D.G. Phipps, J.W. Schumer, J.F. Seely, J.J. Carroll, J.R. Vanhoy, K. Słabkowska, M. Polasik, E. Szymańska, **J. Rzadkiewicz**, **High Energy Density Physics 9** (2013) 500.

[C17] **Ionization energy shift of characteristic K x-ray lines from high-Z materials for plasma diagnostics,** K. Słabkowska, E. Szymanska, M. Polasik, **J. Rzadkiewicz,** et al., **Physics of Plasmas 21**, 031216 (2014).

[C18] **Diagnostics of plasma based on K, L and M x-ray line positions**, K. Słabkowska, E. Szymańska, J. Starosta, M. Polasik, N.R. Pereira, **J. Rzadkiewicz,** M. Kubkowska, A Czarnecka, **Physica Scripta T161**, 014033 (2014).

[C19] **Modeling of the K and L x-ray line structures for molybdenum ions in warm dense Z-pinch plasma**, K. Słabkowska, Ł. Syrocki, E. Szymanska, **J. Rzadkiewicz,** G. Pestka, M. Polasik, **High Energy Density Physics 14** (2015) 44.

[C20] **K X-ray line energies as diagnostics of warm dense plasma**, K. Słabkowska, E. Szymańska, N.R. Pereira, **J. Rzadkiewicz,** Ł. Syrocki, M. Polasik, **High Energy Density Physics 14** (2015) 30.

[C21] **The K X-ray line structures for a warm dense copper plasma**, K. Słabkowska, E. Szymańska, Ł. Syrocki, **J. Rzadkiewicz**, M. Polasik, **High Energy Density Physics 14** (2015) 8.

[C22] **The K x-ray line structures of the 3d-transition metals in warm dense plasma,** E. Szymańska, Ł. Syrocki, K. Słabkowska, M. Polasik, **J. Rzadkiewicz**, **High Energy Density Physics 20** (2016) 29.

[C23] **ITER-relevant calibration technique for soft x-ray spectrometer, J. Rzadkiewicz**, I. Książek, K-D. Zastrow, I. H. Coffey, K. Jakubowska, K. D. Lawson, and JET EFDA Contributors, **Rev. Sci. Instrum. 81**, 10E315 (2010).

[C24] **Determination of metal impurity density, ΔZeff and dilution on JET by VUV emission spectroscopy,** A Czarnecka, K-D Zastrow, **J. Rzadkiewicz**, I. H. Coffey, K. D. Lawson, M. G. O'Mullane and JET-EFDA Contributors, **Plasma Phys. Control. Fusion 53**, 035009 (2011)

[C25] **Determination of tungsten and molybdenum concentrations from an x-ray range spectrum in JET with the ITER-like wall configuration**, T. Nakano, A. E. Shumack, C. F. Maggi, M. Reinke, K. D. Lawson, I. Coffey, T. Pütterich, S. Brezinsek, B. Lipschultz, G. F. Matthews, M. Chernyshova, K. Jakubowska, M. Scholz, **J. Rzadkiewicz**, T. Czarski, W. Dominik, G. Kasprowicz, K. Pozniak, W. Zabolotny, K-D. Zastrow, N. J. Conway**, J. Phys. B: At. Mol. Opt. Phys. 48** (2015) 144023.

[C26] **High performance detectors for upgraded gamma ray diagnostics for JET DT campaigns**, **I. Zychor, G. Bołtruczyk, A. Burakowska, M. Gierlik, M. Gosk, M. Grodzicka-Kobyłka, J. Iwanowska-Hanke, S. Korolczuk, R. Kwiatkowski, S. Mianowski, M. Moszyński, J. Rzadkiewicz, P. Sibczyński, A. Syntfeld-Każuch, Ł. Świderski, M. Szawłowski,**
T. Szczęśniak, J. Szewiński, A. Szydłowski, A. Urban, et al. **Physica Scripta** *91 (2016) 064003.*

[C27] **Digital Approach To High Count Rate Gamma-Ray Spectrometry**, **S. Korolczuk, S. Mianowski**, **J. Rzadkiewicz**, **P. Sibczyński, Ł. Świderski, I. Zychor,** *IEEE Trans. Nucl. Sci. 63 No 3 (2016) 1668.*

[C28] **Characterization of some modern scintillators recommended for use on large fusion facilities in γ-ray spectroscopy and tomographic measurements of γ-emission profiles, P. Sibczyński, A. Brosławski, A. Gójska,** V. Kiptily**, S. Korolczuk, R. Kwiatkowski, S. Mianowski, M. Moszyński, J. Rzadkiewicz, Ł. Świderski, A. Szydłowski, I. Zychor,** *Nukleonika 62 No 3 (2017) 223-228.*

[C29] **Conceptual design of the radial gamma ray spectrometers system for α particle and runaway electron measurements at ITER,** M. Nocente, M. Tardocchi, R. Barnsley, L. Bertalot, B. Brichard, G. Croci, G. Brolatti, L. DiPace, A. Fernandes, L. Giacomelli, I. Lengar, **M. Moszyński**, V. Krasilnikov, A. Muraro, R.C. Pereira, E. PerelliCippo, D. Rigamonti, M. Rebai, **J. Rzadkiewicz**, M. Salewski, P. Santosh, J. Sousa, **I. Zychor**, G. Gorini, *Nucl. Fusion 57 (2017) 076016.*

[C30] **Design of gamma-ray spectrometers optimized for fast particle studies at ITER,** M. Rebai, Bertalot, B. Brichard, G. Brolatti, G. Croci, B. Esposito, A. Fernandes, L. Giacomelli, G. Gorini, V. Krasilnikov, I. Lengar, D. Marocco, A. Muraro, M. Nocente, R. C. Pereira, E. Perelli Cippo, L.D. Rigamonti, **J. Rzadkiewicz**, J. Sousa, and M. Tardocchi, **Rev. Sci. Instrum. 89**, 10I126 (2018).